Aalborg Universitet

AALBORG UNIVERSITY
DENMARK

Speed-Sensorless Control of Induction Motors With an Open-Loop Synchronization Method

Wang, Huimin; Yang, Yongheng; Chen, Dunzhi; Ge, Xinglai ; Li, Songtao; Zuo, Yun

Published in:
IEEE Journal of Emerging and Selected Topics in Power Electronics

DOI (link to publication from Publisher):
10.1109/JESTPE.2021.3050805

Publication date:
2022

Document Version
Accepted author manuscript, peer reviewed version

Link to publication from Aalborg University

Citation for published version (APA):
Wang, H., Yang, Y., Chen, D., Ge, X., Li, S., & Zuo, Y. (2022). Speed-Sensorless Control of Induction Motors With an Open-Loop Synchronization Method. *IEEE Journal of Emerging and Selected Topics in Power Electronics*, *10*(2), 1963-1977. https://doi.org/10.1109/JESTPE.2021.3050805

General rights
Copyright and moral rights for the publications made accessible in the public portal are retained by the authors and/or other copyright owners and it is a condition of accessing publications that users recognise and abide by the legal requirements associated with these rights.

- Users may download and print one copy of any publication from the public portal for the purpose of private study or research.
- You may not further distribute the material or use it for any profit-making activity or commercial gain
- You may freely distribute the URL identifying the publication in the public portal -

Take down policy
If you believe that this document breaches copyright please contact us at vbn@aub.aau.dk providing details, and we will remove access to the work immediately and investigate your claim.

This article has been accepted for publication in a future issue of this journal, but has not been fully edited. Content may change prior to final publication. Citation information: DOI 10.1109/JESTPE.2021.3050805, IEEE Journal of Emerging and Selected Topics in Power Electronics

Speed-Sensorlss Control of Induction Motors with An Open-Loop Synchronization Method

Huimin Wang, *Student Member, IEEE*, Yongheng Yang, *Senior Member, IEEE*, Dunzhi Chen, *Student Member, IEEE*, Xinglai Ge, *Member, IEEE*, Songtao Li, and Yun Zuo

***Abstract*- Speed estimation schemes based on the closed-loop synchronization (CLS) methods for speed-sensorless control of motor drives attract much popularity due to several advantages, e.g., easy implementation, high flexibility, and acceptable performance. However, most of the existing CLS-based estimation schemes may suffer from performance degradation during frequency ramps. Considering this, an attempt of the type-3 phase-locked loop (PLL)-based scheme is made. This solution, however, may adversely affect the system dynamics and stability margin. To address these issues, an open-loop synchronization (OLS) method is proposed for speed-sensorless control of induction motor drives in this paper. In the proposed scheme, the estimated speed is obtained according to the sinusoidal signals and their time-delay signals, rather than increasing the system order. With this, system dynamics and stability margin are maintained. In practice, the disturbance of DC offsets is of concern in induction motor drives. Thus, a closed-loop flux observer is adopted to guarantee the estimation performance under DC offsets. The performance of the proposed OLS scheme is investigated and compared with that of the CLS schemes and the type-3 PLL scheme through experimental tests.**

***Index Terms*-Open-loop synchronization (OLS), speed estimation scheme, closed-loop flux observer, induction motor drives**

I. INTRODUCTION

With strong demands of reliability enhancement and cost reduction, speed-sensorless control becomes increasingly popular in induction motor drives. The procedure involves estimating the speed information properly, and accordingly, removing speed sensors. This task is mostly carried out by using various speed estimation schemes, which can be roughly categorized into non-ideal-phenomena-based and model-based schemes [1], [2]. Poor flexibility and high complexity are two main barriers of the widespread application of the non-ideal-phenomena-based estimation schemes [3], [4].

Manuscript received September 10, 2020; revised November 30, 2020; accepted January 4, 2021. This work was supported by the High-Speed Railway Joint Funds of the National Natural Science Foundation of China (U1934204). (*Corresponding author: Xinglai Ge*.).

H. Wang, X. Ge, S. Li and Y. Zuo are with the Ministry of Education Key Laboratory of Magnetic Suspension Technology and Maglev Vehicle, Southwest Jiaotong University, Chengdu 610031, China (e-mail: wanghuimin@my.swjtu.edu.cn;xlgee@163.com;SongtaoLi@my.swjtu.edu.cn; z _uoy_un@163.com).

Y. Yang is with the Department of Electrical Engineering, Zhejiang University, Hangzhou 310027, China (e-mail: yh.yang@ieee.org)

D. Chen is with the Department of Energy Technology, Aalborg University, Aalborg 9220, Denmark (e-mail: dch@et.aau.dk)

As an alternative, the model-based schemes are highly preferable in speed-sensorless control of induction motor drives. Among model-based estimation methods, schemes using the closed-loop synchronization (CLS) techniques (e.g., phase-locked loop and frequency-locked loop) are of interest, due to being simple and providing satisfactory performance.

As an attractive type of synchronization technique, phase-locked loops (PLLs), which can synchronize the output signals with the input signals, are focused in power and energy applications [5], [6]. Generally, the PLLs behave unsatisfactorily with disturbances due to their insufficient disturbance attenuation capability. As a consequence, the PLL-based estimation schemes may suffer from performance degradation with disturbances (e.g., harmonics, DC offsets, etc) [7]-[12]. For example, an *h*-order harmonic component can result in an (*h*-1)-order ripple in the estimated quantities. To deal with this problem, the PLL-based estimation schemes assisted with different kinds of filters have been recommended in the literature [9]-[12]. More specifically, most of the PLL-based estimation schemes employ a proportional-integral (PI) controller as the loop filter, which makes these schemes lose the ability of accurately tracking frequency ramps. This may present estimation errors in motor drives when the PLL-based schemes operate during acceleration and deceleration processes (i.e., the frequency experiences ramp changes).

Frequency-locked loops (FLLs) are emerged as a type of promising synchronization technique in power and energy applications. Different from the PLLs being implemented in the synchronous reference frame (*dq*-frame), the FLLs generally work in the stationary reference frame (*αβ*-frame) [13]-[17]. The second-order generalized integrator-frequency-locked loop (SOGI-FLL) is one of the notable FLL examples, which has been widely used in single-phase and three-phase grid-synchronization applications [15]-[17]. Similar to the PLL-based estimation schemes, the SOGI-FLL-based estimation schemes achieve unsatisfactory performance during acceleration and deceleration processes for motor drives. The inaccurate estimation of the PLL and the SOGI-FLL schemes during acceleration and deceleration processes may be a concern for induction motor drives. Particularly, this problem may be serious in the applications that require induction motor frequently work in acceleration and deceleration cases. With this, the PLL and the SOGI-FLL schemes are not preferable in terms of estimation accuracy.

Performance improvement during frequency ramps can be attained mainly by two means: increasing the system order and introducing the compensation units. Type-3 PLL-based estimation schemes are typical representatives in terms of

2168-6777 (c) 2020 IEEE. Personal use is permitted, but republication/redistribution requires IEEE permission. See http://www.ieee.org/publications_standards/publications/rights/index.html for more information.
Authorized licensed use limited to: Aalborg Universitetsbibliotek. Downloaded on January 15,2021 at 10:27:43 UTC from IEEE Xplore. Restrictions apply.

This article has been accepted for publication in a future issue of this journal, but has not been fully edited. Content may change prior to final publication. Citation information: DOI 10.1109/JESTPE.2021.3050805, IEEE Journal of Emerging and Selected Topics in Power Electronics

increasing the system order, in which the PI-based LF is replaced by a new LF that has two poles at the origin [18]-[20]. By doing so, this PLL-type estimator can be regarded as a type-3 control system that can resolve the issue of frequency ramps properly. Besides, the increased-order PLL-based schemes including the type-3 enhanced PLL scheme [21], the feedforward-loop PLL scheme [22]-[24], the dual-loop PLL scheme [25]-[27], the steady-state linear Kalman filter-based PLL scheme [28], [29], have also been developed in the literature to tackle the frequency ramp challenge. Though being effective in tracking frequency ramps accurately, the increased-order PLL-based schemes may aggravate stability problem and prolong system dynamics. For example, the type-3 PLL schemes may result in a concern of the negative gain margin. This may increase the risk of system instability. Alternatively, further attempts to improve the estimation performance by introducing additional compensation units into the PLL- and FLL-based estimation schemes are made in [30], [31]. This type of method features with faster dynamics and higher stability margin, compared with the increased-order schemes. However, the presence of extra compensation units increases system complexity with more system parameters, and hence, requires more parameter tuning efforts.

Additionally, the open-loop synchronization (OLS) technique is of growing interest since it cancels the feedback of the estimated quantities, and thus, offers fast dynamics [32]-[37]. Satisfactory estimation can be achieved by using the OLS technique under ideal conditions, while this situation becomes tough when disturbances appear in the inputs. Therefore, the OLS methods accomplish the synchronization task incorporating with various filters to enhance disturbance elimination capability, e.g., the $\alpha\beta$-frame cascaded delayed signal cancellation (CDSC)-based filter [32], [33], the finite-impulse-response (FIR) filter [34], and the moving average filter (MAF) [35]. By doing so, the performance is guaranteed but at the cost of requiring more computational efforts.

In light of the above, in this paper, a speed estimation scheme based on the OLS method (hereafter, referred to as the OLS scheme) is proposed for speed-sensorless control of induction motor drives. The rest of this paper is organized as follows. In Section II, two typical examples of the CLS-based estimation schemes, i.e., the PLL and SOGI-FLL schemes, are briefly introduced, as well as the performance analysis during frequency ramps. To achieve satisfactory estimation accuracy, an attempt of the type-3 PLL scheme is implemented, as presented in Section III. Meanwhile, the properties of the type-3 PLL scheme are also analyzed. The OLS scheme is then elaborated in Section IV. In this scheme, the estimated speed is obtained from the sinusoidal signals and their time-delay signals. It is revealed that the estimation performance is degraded due to the DC offsets. Considering this, a closed-loop flux observer is employed in the OLS scheme in Section V to mitigate the adverse effect of DC offsets. In Section VI, the performance of the OLS scheme is investigated and it is benchmarked with the prior-art CLS schemes and the type-3 PLL scheme through experimental tests. Finally, concluding remarks are provided in Section VII.

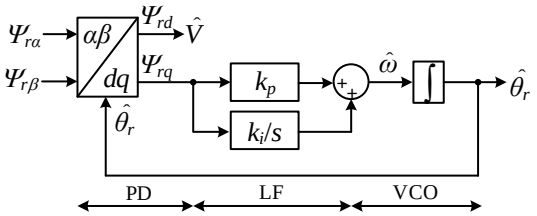

Fig. 1. Block diagram of the PLL scheme (PD: phase detector; LF: loop filter; VCO: voltage-controlled oscillator), in which $\Psi_{r\alpha}$, $\Psi_{r\beta}$, Ψ_{rd}, Ψ_{rq}, k_p, k_i, $\hat{V}$, $\hat{\omega}$, $\hat{\theta}_r$ are α-, β-, d- and q-axis components of the rotor flux (as the inputs), the gains of LF, the estimated amplitude of the rotor flux, the estimated frequency and the estimation of the rotor flux phase, respectively.

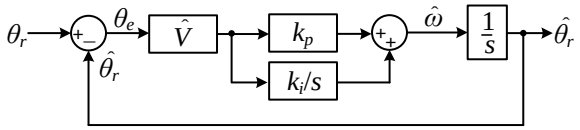

Fig. 2. Small signal model of the PLL scheme, in which θ_r and θ_e are the rotor flux phase and the phase estimation error, respectively.

II. Performance Analysis of the Existing Closed-Loop Synchronization-Based Schemes

A. Performance Analysis of the PLL Scheme

The block diagram of the PLL-based estimation scheme for motor drives is shown in Fig. 1. Here, three parts, e.g., the phase detector (PD), the loop filter (LF), and the voltage-controlled oscillator (VCO), can be found in this scheme [7]-[12]. Also, it can be observed that the inputs of the PLL scheme are rotor flux. To further analyze the performance, the corresponding small signal model of the PLL-based scheme is illustrated in Fig. 2. As mentioned previously, the PLL scheme may present apparent estimation errors when tracking frequency ramps. This is further demonstrated as follows. Based on Fig. 2, the open-loop transfer function $G_{ol}^{PLL}(s)$ can be obtained as

$$G_{ol}^{PLL}(s)=\frac{\hat{\theta}_r}{\theta_r-\hat{\theta}_r}=\frac{\hat{\theta}_r}{\theta_e}=\hat{V}\frac{k_p s+k_i}{s^2} \tag{1}$$

Accordingly, the phase-error transfer function $G_e^{PLL}(s)$ can be given by

$$G_e^{PLL}(s)=\frac{1}{1+G_{ol}^{PLL}(s)}=\frac{s^2}{s^2+\hat{V}k_p s+\hat{V}k_i} \tag{2}$$

When the inputs have a frequency ramp change (h/s^2), corresponding to the phase change (h/s^3), the phase estimation error can be obtained as

$$\Delta\theta_e^{PLL}(s)=\frac{h}{s^3}G_e^{PLL}(s)=\frac{1}{s}\frac{h}{s^2+\hat{V}k_p s+\hat{V}k_i} \tag{3}$$

where h and $\Delta\theta_e^{PLL}$ are the gain of the frequency ramp and the phase estimation error, respectively. Then, the phase estimation error can be calculated by applying the final value theorem. That is,

$$\Delta\theta_{ess}^{PLL}(s)=\lim_{s\to 0}s\Delta\theta_e^{PLL}(s)=\lim_{s\to 0}s\frac{h}{s(s^2+\hat{V}k_p s+\hat{V}k_i)}=\frac{h}{\hat{V}k_i} \tag{4}$$

2168-6777 (c) 2020 IEEE. Personal use is permitted, but republication/redistribution requires IEEE permission. See http://www.ieee.org/publications_standards/publications/rights/index.html for more information.
Authorized licensed use limited to: Aalborg Universitetsbibliotek. Downloaded on January 15,2021 at 10:27:43 UTC from IEEE Xplore. Restrictions apply.

This article has been accepted for publication in a future issue of this journal, but has not been fully edited. Content may change prior to final publication. Citation information: DOI 10.1109/JESTPE.2021.3050805, IEEE Journal of Emerging and Selected Topics in Power Electronics

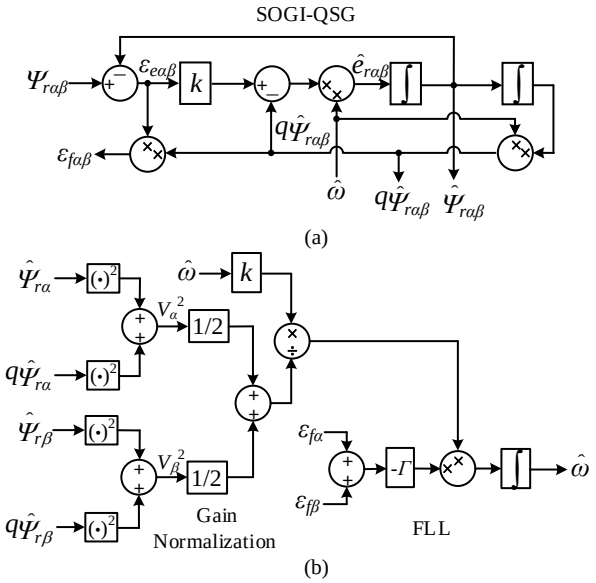

Fig. 3. Block diagram of a typical SOGI-FLL scheme (SOGI-QSG: second-order generalized integrator-based quadrature signal generator; FLL: frequency-locked loop), in which Ψ_r, ε_e, ε_f, $\hat{\omega}$, $\hat{e}_r$, $\hat{\Psi}_r$, $q\hat{\Psi}_r$, k and Γ are the rotor flux (as the inputs), the synchronization error, the frequency error, the estimated frequency, the estimated rotor back electromotive force (EMF), the estimated rotor flux, the quadrature term of the estimated rotor flux, and the gains of the SOGI-FLL scheme, respectively, and α, β indicate the α- and β-axis components of the corresponding variable, respectively: (a) the SOGI-QSG and (b) the FLL with a gain normalization unit.

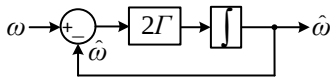

Fig. 4. Simplified model of the FLL scheme.

According to the above analysis, it is indicated that the PLL scheme tracks frequency ramps with an obvious phase estimation error, i.e., (4). The phase estimation error can be mitigated by increasing the PLL bandwidth (i.e., increasing the value of k_i). The disturbance immunity of the high-bandwidth PLL scheme, nevertheless, is degraded.

B. Performance Analysis of the SOGI-FLL Scheme

Fig. 3 presents the block diagram of a typical SOGI-FLL scheme. As seen in Fig. 3, the inputs of the SOGI-FLL scheme are rotor flux signals. And, two SOGI-based quadrature signal generators (SOGI-QSGs) work in parallel to provide the estimated signals of the inputs. Then, a gain normalization unit is adopted to make the SOGI-FLL scheme free from gain variations. Eventually, the FLL is adopted to provide frequency estimation [15], [16].

According to Fig. 3, the frequency characteristic of the SOGI-FLL scheme can be given by [15], [16]

$$\dot{\hat{\omega}} \approx -2\Gamma(\hat{\omega}-\omega) \tag{5}$$

According to (5), the simplified model of the SOGI-FLL scheme can be depicted in Fig. 4. According to Fig. 4, the open-loop transfer function of the SOGI-FLL scheme $G_{ol}^{FLL}(s)$ can be obtained as

$$G_{ol}^{FLL}(s)=\frac{\hat{\omega}}{\omega-\hat{\omega}}=\frac{2\Gamma}{s} \tag{6}$$

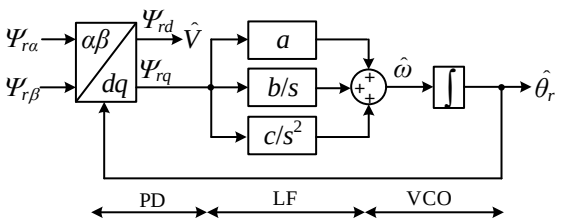

Fig. 5. Block diagram of the type-3 PLL scheme, in which a, b, and c are the gains of the LF.

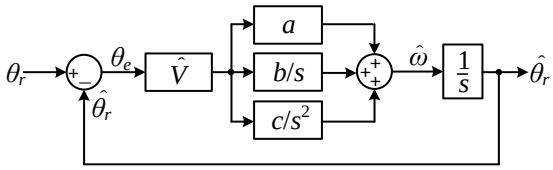

Fig. 6. Small signal model of the type-3 PLL scheme.

Subsequently, the frequency-error transfer function $G_e^{\omega}(s)$ can be given by

$$G_e^{\omega}(s)=\frac{1}{1+G_{ol}^{FLL}(s)}=\frac{s}{s+2\Gamma} \tag{7}$$

When the inputs with a frequency ramp (h/s^2) are applied, and the frequency estimation error can be given by

$$\Delta\omega_e^{FLL}(s)=\frac{h}{s^2}G_e^{\omega}(s)=\frac{h}{s(s+2\Gamma)} \tag{8}$$

According to the final value theorem, the frequency estimation error is calculated as

$$\Delta\omega_{ess}^{FLL}(s)=\lim_{s\to 0}s\Delta\omega_e^{FLL}(s)=\lim_{s\to 0}s\frac{h}{s(s+2\Gamma)}=\frac{h}{2\Gamma}\neq 0 \tag{9}$$

suggesting that an apparent frequency estimation error appears in the SOGI-FLL scheme. Though increasing the value of Γ can reduce frequency estimation error, the dynamics of the SOGI-FLL scheme will be deteriorated [16].

According to the above analysis, the estimation errors appear in the PLL and the SOGI-FLL schemes with frequency ramps. When these schemes are applied in induction motor drives, estimation errors during acceleration and deceleration processes may be observed. This can pose a problem for the applications that require induction motor frequently operate during acceleration and deceleration processes [38].

III. Type-3 PLL Scheme

The type-3 PLL scheme for accurate estimation is presented in this section, in which the performance analysis and dynamics assessment of the type-3 PLL scheme are included.

A. Performance Analysis of the Type-3 PLL Scheme

A typical type-3 PLL scheme is shown in Fig. 5, from which it is known that the main difference between the type-3 PLL scheme and the PLL scheme is the LF [18]-[20]. That is, in the type-3 PLL scheme, the PI-based LF is replaced by a new LF that has two poles at the origin. With this, the entire scheme becomes a type-3 control system that can deal with the frequency ramps properly. Based on Fig. 5, the small signal model of the type-3 PLL scheme is obtained, which is illustrated in Fig. 6. Accordingly, the open-loop transfer

2168-6777 (c) 2020 IEEE. Personal use is permitted, but republication/redistribution requires IEEE permission. See http://www.ieee.org/publications_standards/publications/rights/index.html for more information.
Authorized licensed use limited to: Aalborg Universitetsbibliotek. Downloaded on January 15,2021 at 10:27:43 UTC from IEEE Xplore. Restrictions apply.

This article has been accepted for publication in a future issue of this journal, but has not been fully edited. Content may change prior to final publication. Citation information: DOI 10.1109/JESTPE.2021.3050805, IEEE Journal of Emerging and Selected Topics in Power Electronics

function is obtained as

$$G_{ol}^{TPLL}(s)=\frac{\hat{\theta}_r}{\theta_e}=\frac{\hat{V}(as^2+bs+c)}{s^3} \tag{10}$$

Subsequently, the phase-error transfer function can be obtained as

$$G_e^{TPLL}(s)=\frac{1}{1+G_{ol}^{TPLL}(s)}=\frac{s^3}{s^3+\hat{V}as^2+\hat{V}bs+\hat{V}c} \tag{11}$$

The phase error with frequency ramps can be given by

$$\Delta\theta_e^{TPLL}(s)=\frac{h}{s^3}G_e^{TPLL}(s)=\frac{h}{s^3+\hat{V}as^2+\hat{V}bs+\hat{V}c} \tag{12}$$

Using the final value theorem, it can be calculated as

$$\Delta\theta_{ess}^{TPLL}(s)=\lim_{s\to 0}s\Delta\theta_e^{TPLL}(s)=\lim_{s\to 0}s\frac{h}{s^3+\hat{V}as^2+\hat{V}bs+\hat{V}c}=0 \tag{13}$$

which indicates that the type-3 PLL scheme can track frequency ramps accurately.

B. Dynamics Assessment of the Type-3 PLL Scheme

The accurate estimation during acceleration and deceleration processes is realized by implementing the type-3 PLL scheme at cost of increasing the system order. This, however, may lead to several concerns. A major concern in the type-3 PLL scheme is the negative gain margin. This is further elaborated as follows. The open-loop transfer function of the type-3 PLL scheme (10) can be rewritten as

$$G_{ol}^{TPLL}(s)=\frac{\hat{\theta}_r}{\theta_e}=l\frac{(s+\omega_1)(s+\omega_2)}{s^3} \tag{14}$$

where l, ω_1 and ω_2 are the gains of the LF. To simplify the analysis, considering $\omega_1=\omega_2=\omega_q$, it can be deduced that

$$G_{ol}^{TPLL}(s)=l\frac{(s+\omega_q)^2}{s^3} \tag{15}$$

Accordingly, the amplitude-frequency and the phase-amplitude characteristics of the type-3 PLL scheme can be described as

$$\left|A(j\omega)\right|=\left|G_{ol}^{TPLL}(j\omega)\right|=l\frac{\omega^2+\omega_q{}^2}{\omega^3} \tag{16}$$

$$\varphi=\angle G_{ol}^{TPLL}(j\omega)=2\arctan(\frac{\omega}{\omega_q})-\frac{3}{2}\pi \tag{17}$$

Based on (16) and (17), the phase margin (PM) and the gain margin (GM) of the type-3 PLL scheme can be given by

$$PM=\angle G_{ol}^{TPLL}(j\omega_c)-(-\pi)=2[\arctan(\frac{\omega_c}{\omega_q})]-\frac{1}{2}\pi \tag{18}$$

$$GM=20\lg[\frac{1}{|G_{ol}^{TPLL}(j\omega_g)|}]=20\lg[\frac{\omega_g{}^3}{l(\omega_g{}^2+\omega_q{}^2)}] \tag{19}$$

with ω_c and ω_g being the amplitude crossing frequency and the phase crossing frequency, respectively. Moreover, it can be obtained as

$$\left|G_{ol}^{TPLL}(j\omega_c)\right|=1 \tag{20}$$

$$\angle G_{ol}^{TPLL}(j\omega_g)=-\pi \tag{21}$$

Then,

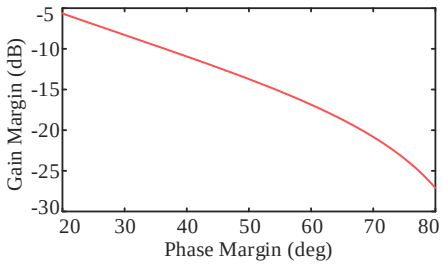

Fig. 7. Relationship between the gain margin (PM) and the phase margin (PM) of the type-3 PLL scheme.

$$l\frac{\omega_c{}^2+\omega_q{}^2}{\omega_c{}^3}=1 \tag{22}$$

$$\omega_g=\omega_q \tag{23}$$

(18) can be rewritten as

$$PM=2[\arctan(\frac{\omega_c}{\omega_q})]-\frac{1}{2}\pi=2\varphi_q-\frac{1}{2}\pi \tag{24}$$

Then,

$$\tan(\varphi_q)=\frac{\omega_c}{\omega_q} \tag{25}$$

Based on (24), it can be deduced that

$$\tan(PM)+\sec(PM)=\tan\varphi_q \tag{26}$$

Substituting (26) into (25) gives

$$\frac{\omega_q}{\omega_c}=\frac{1}{\tan(PM)+\sec(PM)} \tag{27}$$

According to (25), it can be obtained as

$$\sin(\varphi_q)=\frac{\omega_c}{\sqrt{\omega_q{}^2+\omega_c{}^2}} \tag{28}$$

Substituting (28) into (22) gives

$$\frac{\omega_c}{l}=\frac{1}{(\sin\varphi_q)^2} \tag{29}$$

According to (24), it can be obtained that

$$\sin(PM)+1=\sin(2\varphi_q-\frac{1}{2}\pi)+1=2[\sin(\varphi_q)]^2 \tag{30}$$

Subsequently,

$$\frac{\omega_c}{l}=\frac{2}{\sin(PM)+1} \tag{31}$$

Based on (23), (27) and (31), the GM can be rewritten as

$$\begin{aligned}GM&=20\lg[\frac{\omega_g{}^3}{l(\omega_g{}^2+\omega_q{}^2)}]=20\lg(\frac{\omega_q}{2l})=20\lg(\frac{\omega_q}{\omega_c}\times\frac{\omega_c}{2l})\\&=20\lg[\frac{1}{\tan(PM)+\sec(PM)}\times\frac{1}{\sin(PM)+1}]\\&=20\lg\{\frac{\cos(PM)}{[\sin(PM)+1]^2}\}\end{aligned} \tag{32}$$

Observations in (32) indicate that the GM of the type-3 PLL scheme is highly related to the PM. The PM of the type-3 PLL scheme is reasonable within the range from 40°-50°. Due to this, the GM of the type-3 PLL scheme is negative, as shown in Fig. 7. The negative GM may aggravate the stability

2168-6777 (c) 2020 IEEE. Personal use is permitted, but republication/redistribution requires IEEE permission. See http://www.ieee.org/publications_standards/publications/rights/index.html for more information.
Authorized licensed use limited to: Aalborg Universitetsbibliotek. Downloaded on January 15,2021 at 10:27:43 UTC from IEEE Xplore. Restrictions apply.

This article has been accepted for publication in a future issue of this journal, but has not been fully edited. Content may change prior to final publication. Citation information: DOI 10.1109/JESTPE.2021.3050805, IEEE Journal of Emerging and Selected Topics in Power Electronics

problem in the type-3 PLL scheme [30]. Furthermore, the type-3 PLL scheme increases the system order with more parameters. Therefore, this scheme may affect system dynamics and require more parameters tuning efforts.

IV. Open-Loop Synchronization Scheme

From the aforementioned analysis, the existing CLS-based estimation schemes (e.g., PLL- and SOGI-FLL-based schemes) may not provide accurate estimation during acceleration and deceleration processes. Additionally, though being effective to improve estimation performance during acceleration and deceleration processes, the type-3 PLL scheme may result in new concerns in the estimation scheme, e.g., negative gain margin and degraded dynamics. Considering this, an OLS scheme is presented in this section, in which the estimated frequency is provided from the inputs and their time-delay signals, rather than increasing the system order.

A. OLS Scheme Under Ideal Condition

Assuming the inputs of the OLS scheme (i.e., rotor flux) are purely sinusoidal signals with unity amplitudes under ideal conditions:

$$\begin{cases} \Psi_{r\alpha}(t) = \cos(\omega t + \varphi) \\ \Psi_{r\beta}(t) = \sin(\omega t + \varphi) \end{cases} \tag{33}$$

in which ω and φ are the frequency and the initial phase of the rotor flux. (33) can be rewritten in the discrete form, as

$$\begin{cases} \Psi_{r\alpha}(k) = \cos(k\omega T_s + \varphi) \\ \Psi_{r\beta}(k) = \sin(k\omega T_s + \varphi) \end{cases} \tag{34}$$

where T_s is the sampling time. Applying a time delay to the inputs gives

$$\begin{cases} \Psi_{r\alpha}(k-\tau) = \cos[\omega(kT_s - \tau) + \varphi] \\ \Psi_{r\beta}(k-\tau) = \sin[\omega(kT_s - \tau) + \varphi] \end{cases} \tag{35}$$

where τ is the delay time. Subsequently, it can be obtained that

$$\begin{cases} \Psi_{r\alpha}(k-\tau) = \cos(k\omega T_s + \varphi)\cos(\omega\tau) + \sin(k\omega T_s + \varphi)\sin(\omega\tau) \\ \Psi_{r\beta}(k-\tau) = \sin(k\omega T_s + \varphi)\cos(\omega\tau) - \cos(k\omega T_s + \varphi)\sin(\omega\tau) \end{cases} \tag{36}$$

Based on (34) and (35), it can be deduced that

$$\cos(\omega\tau) = \Psi_{r\alpha}(k-\tau)\Psi_{r\alpha}(k) + \Psi_{r\beta}(k-\tau)\Psi_{r\beta}(k) \tag{37}$$

Then, the estimated frequency can be obtained as

$$\omega = \frac{\arccos[\Psi_{r\alpha}(k-\tau)\Psi_{r\alpha}(k) + \Psi_{r\beta}(k-\tau)\Psi_{r\beta}(k)]}{\tau} \tag{38}$$

which shows that the estimated frequency is obtained based on the sinusoidal signals. Compared with the type-3 PLL scheme, the OLS scheme without increasing the system order is a more promising option in terms of acceptable dynamics and high stability margin.

B. OLS Scheme with Distorted Inputs

In the ideal condition (i.e., the inputs are free from disturbances), the OLS scheme can achieve satisfactory estimation. However, this situation is not always true because disturbances will inevitably appear in the inputs in practice. When considering the presence of distortions, the inputs of the OLS scheme can be expressed as

$$\begin{cases} \Psi_{r\alpha h}(t) = \cos(\omega t + \varphi) + \delta_{h\alpha}(t) \\ \Psi_{r\beta h}(t) = \sin(\omega t + \varphi) + \delta_{h\beta}(t) \end{cases} \tag{39}$$

where $\delta_{h\alpha}(t)$ and $\delta_{h\beta}(t)$ are the distortion components, respectively. The same method is applied, and it can be obtained that

$$\Psi_{r\alpha h}(k-\tau)\Psi_{r\alpha h}(k) + \Psi_{r\beta h}(k-\tau)\Psi_{r\beta h}(k) = \cos(\omega\tau) + H(k) \tag{40}$$

Here, $H(k)$ is the disturbance component considering the effect of distortions, and it can be described as

$$H(k) = h_1(k) + h_2(k) + h_3(k) + h_4(k) + h_5(k) + h_6(k) \tag{41}$$

with,

$$\begin{cases} h_1(k) = [\cos(k\omega T_s + \varphi)\cos(\omega\tau) + \sin(k\omega T_s + \varphi)\sin(\omega\tau)]\delta_{h\alpha}(k) \\ h_2(k) = \cos(k\omega T_s + \varphi)\delta_{h\alpha}(k-\tau) \\ h_3(k) = \delta_{h\alpha}(k-\tau)\delta_{h\alpha}(k) \\ h_4(k) = [\sin(k\omega T_s + \varphi)\cos(\omega\tau) - \cos(k\omega T_s + \varphi)\sin(\omega\tau)]\delta_{h\beta}(k) \\ h_5(k) = \sin(k\omega T_s + \varphi)\delta_{h\beta}(k-\tau) \\ h_6(k) = \delta_{h\beta}(k-\tau)\delta_{h\beta}(k) \end{cases}$$

Eventually, the estimated frequency when considering the effect of distortions can be given by

$$\begin{aligned} \omega_h &= \frac{\arccos[\Psi_{r\alpha h}(k-\tau)\Psi_{r\alpha h}(k) + \Psi_{r\beta h}(k-\tau)\Psi_{r\beta h}(k)]}{\tau} \\ &= \frac{\arccos[\cos(\omega\tau) + H(k)]}{\tau} \end{aligned} \tag{42}$$

where ω_h is the estimated frequency with distorted inputs. According to (42), when the inputs are distorted, the estimation performance of the OLS scheme experiences obvious performance degradation.

C. OLS Scheme with A Robust Adaptive Law

When distortions appear in the inputs, the estimation performance of the OLS scheme is degraded. To address this, a robust adaptive law is adopted in the OLS scheme. This is further elaborated as follows. Considering a linear parametric model with model errors, that is

$$\boldsymbol{\xi}(t) = \boldsymbol{G}^{*T}\boldsymbol{\chi}(t) - \boldsymbol{\kappa}(t) \tag{43}$$

where $\boldsymbol{G}^{*T} \in \boldsymbol{R}^n$ ($\boldsymbol{R}$ means the set of real number) is an unknown parameter vector, $\boldsymbol{\xi}(t) \in \boldsymbol{R}$ is a measured vector, $\boldsymbol{\chi}(t) \in \boldsymbol{R}^n$ is a known parameter vector, $\boldsymbol{\kappa}(t)$ is the model system errors, respectively. Let $\boldsymbol{G}^T$ be the estimated value of $\boldsymbol{G}^{T*}$ and define the estimation error as

$$\boldsymbol{\tau}(t) = \boldsymbol{G}^T\boldsymbol{\chi}(t) - \boldsymbol{G}^{T*}\boldsymbol{\chi}(t) \tag{44}$$

A standard gradient algorithm is used to update the estimation of $\boldsymbol{G}^{T*}$. That is, the cost function is defined as

$$\boldsymbol{J} = \frac{\boldsymbol{\tau}^2}{2m^2} = \frac{\tilde{\boldsymbol{G}}^T\boldsymbol{\chi}(t)\boldsymbol{\chi}^T(t)\tilde{\boldsymbol{G}}}{2m^2} \tag{45}$$

where $\tilde{\boldsymbol{G}}^T = \boldsymbol{G}^T - \boldsymbol{G}^{T*}$ and m is a normalized signal which is independent on $\boldsymbol{G}^T$. Accordingly, it can be given by

2168-6777 (c) 2020 IEEE. Personal use is permitted, but republication/redistribution requires IEEE permission. See http://www.ieee.org/publications_standards/publications/rights/index.html for more information.
Authorized licensed use limited to: Aalborg Universitetsbibliotek. Downloaded on January 15,2021 at 10:27:43 UTC from IEEE Xplore. Restrictions apply.

This article has been accepted for publication in a future issue of this journal, but has not been fully edited. Content may change prior to final publication. Citation information: DOI 10.1109/JESTPE.2021.3050805, IEEE Journal of Emerging and Selected Topics in Power Electronics

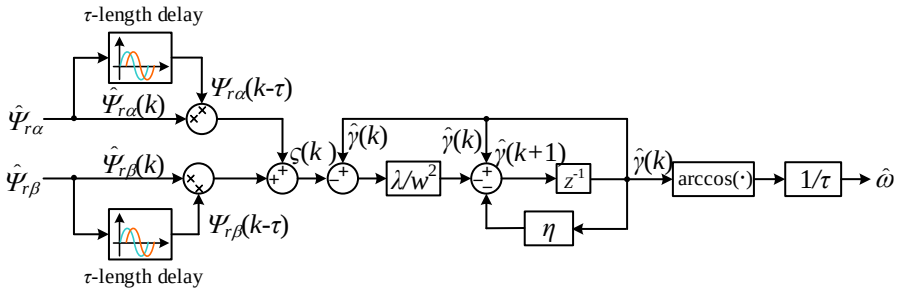

Fig. 8. Block diagram of the OLS scheme with a robust adaptive law.

$$\frac{d}{dt}\boldsymbol{G}^{\boldsymbol{T}} = -\boldsymbol{\Gamma}\frac{d\boldsymbol{J}}{d\boldsymbol{\tau}}\frac{d\boldsymbol{\tau}}{d\boldsymbol{G}^{\boldsymbol{T}}} = -\boldsymbol{\Gamma}\frac{\boldsymbol{\tau}}{m^2}\boldsymbol{\chi}(t) \tag{46}$$

where $\boldsymbol{\Gamma}$ is a gain matrix and $\boldsymbol{\Gamma} = \boldsymbol{\Gamma}^{\boldsymbol{T}} > 0$. Moreover, m can be described as

$$m = \sqrt{\upsilon + \boldsymbol{\chi}^{\boldsymbol{T}}(t)\boldsymbol{\chi}(t)} \tag{47}$$

with υ being a designed parameter. When considering the effect of the system errors $\boldsymbol{\kappa}(t)$ in (43), the estimation error should be re-defined as

$$\boldsymbol{\varepsilon}(t) = \tilde{\boldsymbol{G}}^{\boldsymbol{T}}\boldsymbol{\chi}(t) + \boldsymbol{\kappa}(t) \tag{48}$$

Accordingly, the estimation of $\boldsymbol{G}^{\boldsymbol{T}*}$ should be modified as

$$\frac{d}{dt}\boldsymbol{G}^{\boldsymbol{T}} = -\boldsymbol{\Gamma}\frac{\boldsymbol{\tau}}{m^2}\boldsymbol{\chi}(t) + \boldsymbol{f}(t) \tag{49}$$

where $\boldsymbol{f}(t)$ is a modification term for robustness with respect to model errors $\boldsymbol{\kappa}(t)$. A so-called σ-modification method is used to obtain the robustness [39], which is given by

$$\boldsymbol{f}(t) = -\boldsymbol{\sigma}\boldsymbol{G}^{\boldsymbol{T}} \tag{50}$$

in which $\boldsymbol{\sigma}>0$ is a constant designed parameter. Then, the modified estimation of $\boldsymbol{G}^{\boldsymbol{T}*}$ can be obtained as

$$\frac{d}{dt}\boldsymbol{G}^{\boldsymbol{T}} = -\boldsymbol{\Gamma}\frac{\boldsymbol{\tau}}{m^2}\boldsymbol{\chi}(t) - \boldsymbol{\sigma}\boldsymbol{G}^{\boldsymbol{T}} \tag{51}$$

Then, the discrete form of (51) can be written as

$$\boldsymbol{G}^{\boldsymbol{T}}(k+1) - \boldsymbol{G}^{\boldsymbol{T}}(k) = -\boldsymbol{\Gamma}\frac{\boldsymbol{\tau}(k)}{m^2}\boldsymbol{\chi}(k) - \boldsymbol{\sigma}\boldsymbol{G}^{\boldsymbol{T}}(k) \tag{52}$$

Finally, it can be obtained that

$$\boldsymbol{G}^{\boldsymbol{T}}(k+1) = \boldsymbol{G}^{\boldsymbol{T}}(k) - \boldsymbol{\Gamma}\frac{\boldsymbol{\tau}(k)}{m^2}\boldsymbol{\chi}(k) - \boldsymbol{\sigma}\boldsymbol{G}^{\boldsymbol{T}}(k) \tag{53}$$

According to the above analysis, the OLS scheme with a robust adaptive law is used, and the output error is defined as

$$\varsigma(k) = \cos(\hat{\omega}\tau) - [\Psi_{r\alpha h}(k-\tau)\Psi_{r\alpha h}(k) + \Psi_{r\beta h}(k-\tau)\Psi_{r\beta h}(k)] \tag{54}$$

where $\varsigma(k)$ is the output error. Substituting (40) into (54) yields

$$\varsigma(k) = \underbrace{\cos(\hat{\omega}\tau)}_{\hat{\gamma}} - \underbrace{\cos(\omega\tau)}_{\gamma} - H(k) = \varsigma_{\gamma}(k) - H(k) \tag{55}$$

To accurately estimate the term of $\cos(\omega\tau)$, a robust adaptive law in (53) is employed as

$$\hat{\gamma}(k+1) = \hat{\gamma}(k) - \frac{\lambda\varsigma(k)}{w^2} + X(k) \tag{56}$$

where λ and w are the gains of the control system, $X(k)$ is the modification term for robustness with respect to $H(k)$, and $X(k)$ can be designed as

$$X(k) = -\eta\hat{\gamma}(k) \tag{57}$$

with η being the adaptation gain, and $\eta \in (0,\ 0.5)$. Then, the estimated frequency can be obtained as

$$\hat{\omega} = \frac{\arccos[\hat{\gamma}(k)]}{\tau} \tag{58}$$

According to the above analysis, the block diagram of the OLS scheme with a robust adaptive law is presented in Fig. 8.

D. Performance Analysis of the OLS Scheme

Additionally, the impact of the DC offsets on different schemes is explored, and the results are presented in Fig. 9. As expected, the performance of the CLS-based schemes is worsened because of the DC offset in inputs. More specifically, the DC offset causes large oscillations in the estimated phase and frequency [see Figs. 9(a) and 9(b)]. Unfortunately, this situation also occurs in the OLS scheme. As shown in Fig. 9(c), oscillatory ripples appear in the OLS scheme due to DC offsets. In motor drives, the DC offset is often inevitable in the measured signals. Therefore, further efforts should be made to remove the effect of DC offsets, considering the application of the OLS scheme for induction motor drives.

V. Speed Estimation Scheme Based on the OLS Method

The implementation of the OLS scheme for speed-sensorless-controlled induction motor drives is detailed in this section, in which the DC offsets will be addressed by using a closed-loop flux observer.

A. Practical Implementation of the OLS Scheme

The practical implementation of the OLS scheme is depicted in Fig. 10. As shown, several units, e.g., a closed-loop flux observer, an amplitude normalization (AN) unit, and the OLS-based scheme, can be observed. The closed-loop flux observer is mainly responsible for providing the estimated rotor flux and robustness against the DC offsets. After the AN stage, the estimated rotor flux is used as the inputs of the OLS scheme. Then, the estimated frequency can be calculated through the OLS scheme. In addition, the estimated rotor flux phase (which is used as the flux-orientation phase) and the estimated slip frequency (which is used for the calculation of the rotor speed) are obtained from the closed-loop flux observer. Eventually, the estimated rotor speed is calculated as

2168-6777 (c) 2020 IEEE. Personal use is permitted, but republication/redistribution requires IEEE permission. See http://www.ieee.org/publications_standards/publications/rights/index.html for more information.
Authorized licensed use limited to: Aalborg Universitetsbibliotek. Downloaded on January 15,2021 at 10:27:43 UTC from IEEE Xplore. Restrictions apply.

This article has been accepted for publication in a future issue of this journal, but has not been fully edited. Content may change prior to final publication. Citation information: DOI 10.1109/JESTPE.2021.3050805, IEEE Journal of Emerging and Selected Topics in Power Electronics

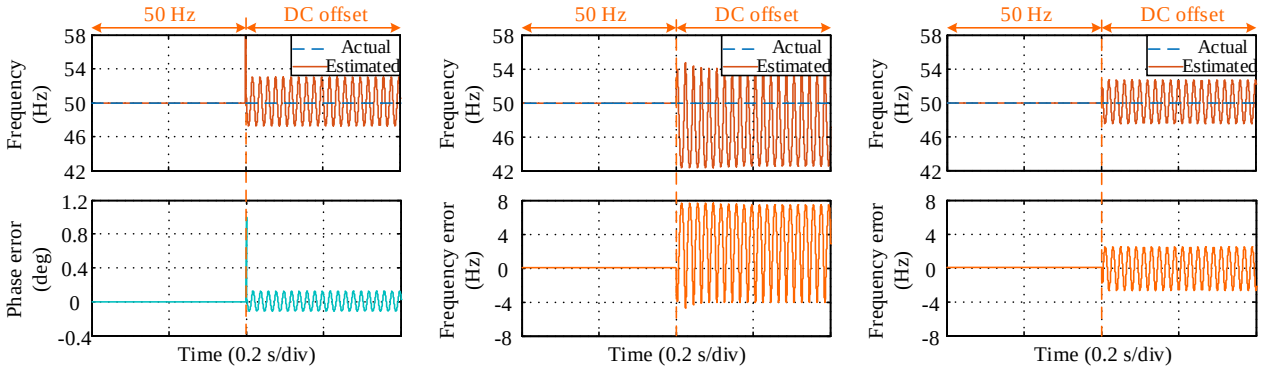

Fig. 9. Estimation performance of different schemes with a DC offset of +1 A: (a) the PLL scheme, (b) the SOGI-FLL scheme, and (c) the OLS scheme.

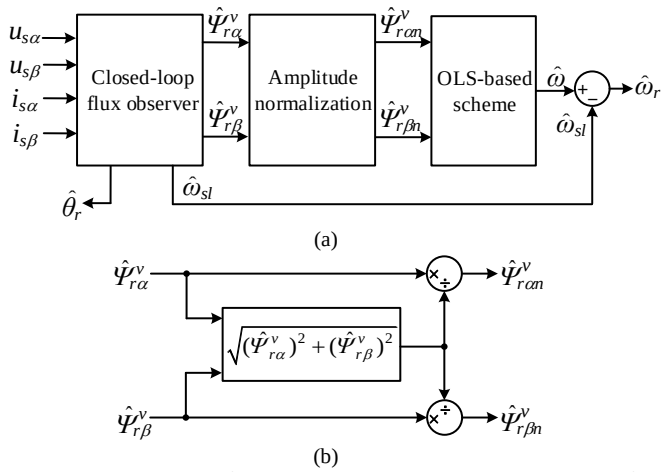

Fig. 10. Implementation of the OLS scheme, in which a closed-loop flux observer is used to address the issue of DC offsets: (a) the block diagram of the OLS scheme and (b) the block diagram of the amplitude normalization.

$$\hat{\omega}_r = \hat{\omega} - \hat{\omega}_{sl} \tag{59}$$

where $\hat{\omega}$, $\hat{\omega}_r$ and $\hat{\omega}_{sl}$ are the estimated frequency provided by the OLS scheme, the estimated rotor speed and the estimated slip frequency from the closed-loop flux observer. And,

$$\hat{\omega}_{sl} = \frac{R_r(\hat{\Psi}^v_{s\alpha} i_{s\beta} - \hat{\Psi}^v_{s\beta} i_{s\alpha})}{\left|\hat{\Psi}^v_r\right|^2} \tag{60}$$

in which $\hat{\Psi}^v_{s\alpha}$, $\hat{\Psi}^v_{s\alpha}$, $\left|\hat{\Psi}^v_r\right|$ and R_r are the α- and β-axis components of the estimated stator flux, the estimated rotor flux amplitude and the rotor resistance, respectively.

B. Closed-Loop Flux Observer

In the implementation of the OLS scheme, a closed-loop flux observer is adopted to enhance the robustness against the DC offsets, which is illustrated in Fig. 11. In Fig. 11, $u_{s\alpha\beta}$, $i_{s\alpha\beta}$, $\Psi_{s\alpha\beta}{}^i$, $\Psi_{r\alpha\beta}{}^i$, $\hat{\Psi}^v_{s\alpha\beta}$, $\hat{\Psi}^v_{r\alpha\beta}$, $\hat{\theta}_r$ and R_s are the stator voltage vector, the stator current vector, the stator flux vector in the current model (CM), the rotor flux vector in the CM, the estimated stator flux vector in the voltage model (VM), the estimated rotor flux vector in the VM, the estimated rotor flux phase and the stator resistance, correspondingly.

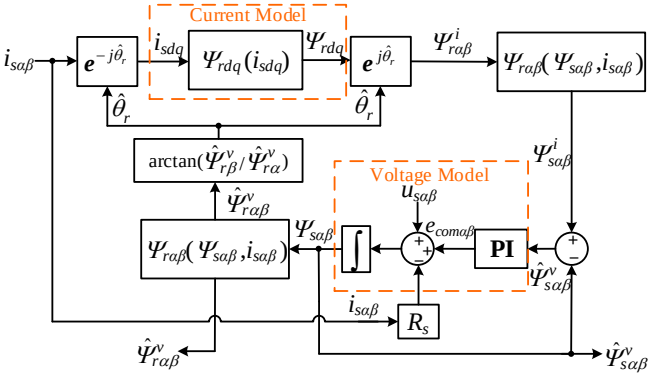

Fig. 11. Block diagram of the closed-loop flux observer.

The closed-loop flux observer is considered as the adaptive combination of two common flux observers (i.e., VM- and CM-based flux observers). It can be accepted as a model reference adaptive system and the two open-loop flux observers are regulated together by a PI controller. By doing so, the closed-loop flux observer is expected to be able to tackle the challenge of DC offsets [40]. The closed-loop flux observer is analyzed as follows. The VM- and the CM-based flux observer in the $\alpha\beta$-frame are expressed as

$$\begin{cases} \begin{bmatrix} \Psi^v_{s\alpha} \\ \Psi^v_{s\beta} \end{bmatrix} = \begin{bmatrix} \int e_{s\alpha} \\ \int e_{s\beta} \end{bmatrix} = \begin{bmatrix} \int (u_{s\alpha} - R_s i_{s\alpha}) \\ \int (u_{s\beta} - R_s i_{s\beta}) \end{bmatrix} \\ \begin{bmatrix} \Psi^v_{r\alpha} \\ \Psi^v_{r\beta} \end{bmatrix} = \begin{bmatrix} \frac{L_r}{L_m}\Psi^v_{s\alpha} - \frac{L_s L_r - L_m{}^2}{L_m} i_{s\alpha} \\ \frac{L_r}{L_m}\Psi^v_{s\beta} - \frac{L_s L_r - L_m{}^2}{L_m} i_{s\beta} \end{bmatrix} \end{cases} \tag{61}$$

$$\begin{cases} \Psi^i_{r\alpha} = \int \left(-\frac{1}{T_r}\Psi^i_{r\alpha} - \omega_r \Psi^i_{r\beta} + \frac{L_m}{T_r} i_{s\alpha} \right) \\ \Psi^i_{r\beta} = \int \left(\omega_r \Psi^i_{r\alpha} - \frac{1}{T_r}\Psi^i_{r\beta} + \frac{L_m}{T_r} i_{s\beta} \right) \end{cases} \tag{62}$$

where $e_{s\alpha}$, $e_{s\beta}$, L_s, L_r, L_m, T_r and ω_r are the α- and β-axis components of the stator back electromotive force signals (EMFs), the stator inductance, the rotor inductance, the magnetizing inductance, the rotor time constant and the rotor

2168-6777 (c) 2020 IEEE. Personal use is permitted, but republication/redistribution requires IEEE permission. See http://www.ieee.org/publications_standards/publications/rights/index.html for more information.
Authorized licensed use limited to: Aalborg Universitetsbibliotek. Downloaded on January 15,2021 at 10:27:43 UTC from IEEE Xplore. Restrictions apply.

This article has been accepted for publication in a future issue of this journal, but has not been fully edited. Content may change prior to final publication. Citation information: DOI 10.1109/JESTPE.2021.3050805, IEEE Journal of Emerging and Selected Topics in Power Electronics

speed, respectively. Moreover, $T_r = L_r/R_r$. Based on (62), the CM in the *dq*-frame can be represented as

$$\begin{cases} \Psi_{rd}^{i} = \int\left[-\frac{1}{T_r}\Psi_{rd}^{i} + (\omega_s - \omega_r)\Psi_{rq}^{i} + \frac{L_m}{T_r} i_{sd}\right] \\ \Psi_{rq}^{i} = \int\left[-(\omega_s - \omega_r)\Psi_{rd}^{i} - \frac{1}{T_r}\Psi_{rq}^{i} + \frac{L_m}{T_r} i_{sq}\right] \end{cases} \tag{63}$$

In the rotor flux-orientation control system, the rotor flux in the *dq*-frame can be described as

$$\begin{cases} \Psi_{rd} = |\Psi_r| \\ \Psi_{rq} = 0 \end{cases} \tag{64}$$

in which $|\Psi_r|$ is the amplitude of rotor flux. Substituting (64) into (63), and the CM in the *dq*-frame can be rewritten as

$$\begin{cases} \Psi_{rd}^{i} = |\Psi_r| = \frac{L_m}{1+pT_r} i_{sd} \\ \Psi_{rq}^{i} = 0 \end{cases} \tag{65}$$

with p being the differential operator. Then, the stator flux provided by the CM can be obtained as

$$\begin{bmatrix} \Psi_{s\alpha}^{i} \\ \Psi_{s\beta}^{i} \end{bmatrix} = \frac{L_s L_r - L_m^{\,2}}{L_r} \begin{bmatrix} i_{s\alpha} \\ i_{s\beta} \end{bmatrix} + \frac{L_m}{L_r} \begin{bmatrix} \Psi_{r\alpha}^{i} \\ \Psi_{r\beta}^{i} \end{bmatrix} \tag{66}$$

In order to alleviate the effect of the DC offsets, a DC-offset compensation term $e_{com\beta}$ is adopted in the VM:

$$\begin{bmatrix} \hat{\Psi}_{s\alpha}^{v} \\ \hat{\Psi}_{s\beta}^{v} \end{bmatrix} = \begin{bmatrix} \int (u_{s\alpha} - R_s i_{s\alpha} + e_{com\alpha}) \\ \int (u_{s\beta} - R_s i_{s\beta} + e_{com\beta}) \end{bmatrix} \tag{67}$$

And, the compensation unit of the DC offsets can be realized by

$$\begin{bmatrix} e_{com\alpha} \\ e_{com\beta} \end{bmatrix} = \underbrace{\left(k_{po} + \frac{k_{io}}{s}\right)}_{PI} \begin{bmatrix} \Psi_{s\alpha}^{i} - \hat{\Psi}_{s\alpha}^{v} \\ \Psi_{s\beta}^{i} - \hat{\Psi}_{s\beta}^{v} \end{bmatrix} \tag{68}$$

in which k_{po} and k_{io} are the gains of the compensation unit. Eventually, the estimated rotor flux can be given as

$$\begin{bmatrix} \hat{\Psi}_{r\alpha}^{v} \\ \hat{\Psi}_{r\beta}^{v} \end{bmatrix} = -\frac{L_s L_r - L_m^{\,2}}{L_m} \begin{bmatrix} i_{s\alpha} \\ i_{s\beta} \end{bmatrix} + \frac{L_r}{L_m} \begin{bmatrix} \hat{\Psi}_{s\alpha}^{v} \\ \hat{\Psi}_{s\beta}^{v} \end{bmatrix} \tag{69}$$

Moreover, the estimated rotor flux phase can be calculated as

$$\hat{\theta}_r = \arctan\left(\frac{\hat{\Psi}_{r\beta}^{v}}{\hat{\Psi}_{r\alpha}^{v}}\right) \tag{70}$$

In addition to providing good immunity to DC offsets, it is worth noting that the estimated speed is not fed back into the closed-loop flux observer, and thus, this observer is insensitive to speed estimation errors. Moreover, the rotor flux estimation of this observer can mitigate the lagging effect of the speed estimation.

Simulations are performed to investigate the performance of the closed-loop flux observer, and the performance of the VM-based flux observer is also provided as a comparison, which can be found in Fig. 12. In this case, the reference value of rotor flux in induction motor drives and the DC offset are set to 1.13 Wb and 0.5 V, respectively.

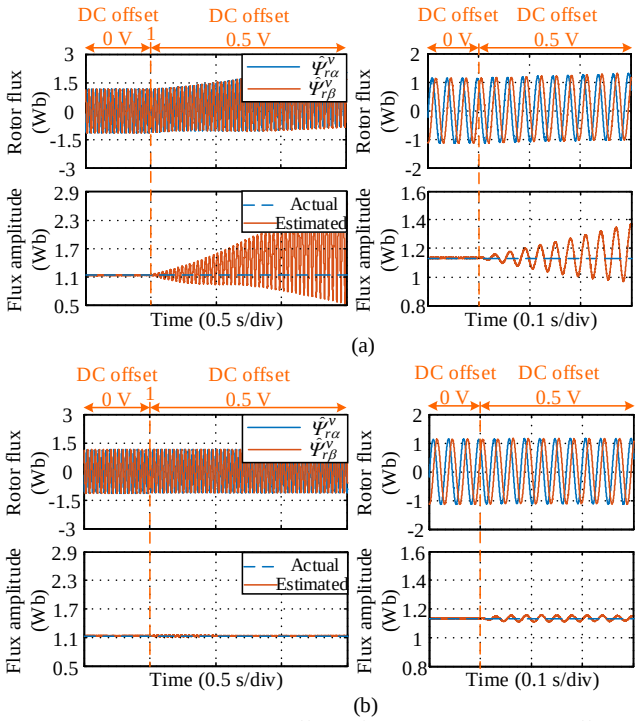

Fig. 12. Flux estimation by using different flux observers with DC offsets: (a) the VM-based flux observer and (b) the closed-loop flux observer.

TABLE I
PARAMETERS OF THE INDUCTION MOTOR

Parameter	Value	Parameter	Value
Rated Power (kW)	2.2	Stator resistance (Ω)	3.67
Rated voltage (V)	220	Rotor resistance (Ω)	2.32
Rated current (A)	5.1	Stator inductance (mH)	244.2
Phase	3	Rotor inductance (mH)	247.3
Pole pairs	2	Magnetizing inductance (mH)	235

As shown in Fig. 12(a), serious distortions occur in the estimated rotor flux when the DC offset is introduced into the VM-based flux observer. Meanwhile, the disturbance of the DC offsets causes obvious ripples in the amplitude of estimated rotor flux. However, the estimated rotor flux provided by the closed-loop observer makes a considerable performance enhancement with the disturbance of DC offsets. That is, no obvious distortions appear in the estimated rotor flux and the growing oscillations in the amplitude of estimated rotor flux are absent [see Fig. 12(b)]. According to the performance comparison, it is evident that the closed-loop flux observer is a good option to attenuate the DC offsets.

VI. Experimental Results

To validate the effectiveness of the OLS scheme, experimental tests are carried out referring to the block diagram of the entire speed-sensorless-controlled induction motor drives in Fig. 13. The experiment set-up is shown in Fig. 14, which consists of a Danfoss FC302 inverter, a 2.2-kW induction motor, a mechanically coupled load surface-mounted permanent-magnet synchronous motor (SPMSM) and a dSPACE 1103. The parameters of the induction motor are listed in Table I.

2168-6777 (c) 2020 IEEE. Personal use is permitted, but republication/redistribution requires IEEE permission. See http://www.ieee.org/publications_standards/publications/rights/index.html for more information.
Authorized licensed use limited to: Aalborg Universitetsbibliotek. Downloaded on January 15,2021 at 10:27:43 UTC from IEEE Xplore. Restrictions apply.

This article has been accepted for publication in a future issue of this journal, but has not been fully edited. Content may change prior to final publication. Citation information: DOI 10.1109/JESTPE.2021.3050805, IEEE Journal of Emerging and Selected Topics in Power Electronics

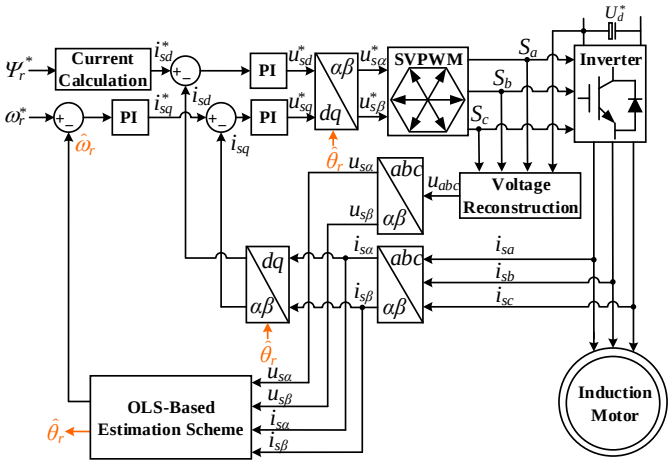

Fig. 13. Block diagram of the speed-sensorless-controlled induction motor drives (SVPWM- Space vector pulse-width modulation).

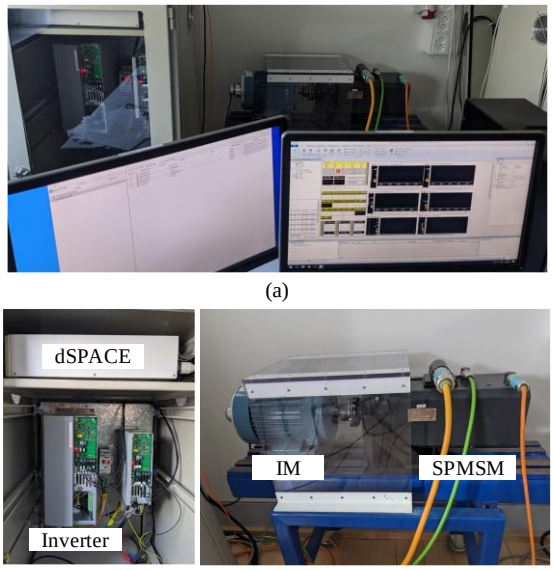

(a)

(b)

Fig. 14. Experimental set-up system: (a) the entire induction motor drives and (b) the inverter and induction motor drives.

The performance of the OLS scheme under speed command variations is firstly presented in Fig. 15. In this case, the speed command is changed from 1000 r/min to 1300 r/min, and then decreases to 1100 r/min. As shown in Fig. 15, when enabling the OLS scheme, the estimated speed makes a good agreement with the actual speed, and accordingly, the estimation error is within a reasonable range. Meanwhile, the performance of the SOGI-FLL scheme is provided as a comparison, which is illustrated in Fig. 16. To make a fair comparison, the test case of the SOGI-FLL scheme is the same as that in Fig. 15. Observations in Fig. 16 indicate that the SOGI-FLL scheme behaves unsatisfactorily during acceleration and deceleration processes. That is, obvious estimation errors can be observed. This situation, however, can be effectively mitigated by implementing the OLS scheme. Additionally, the estimated rotor flux phase provided by the OLS scheme works well in the entire speed range, as shown in Fig. 17.

The performance of the OLS scheme in response to load variations is also investigated, and the corresponding results are depicted in Fig. 18. In this case, the load is varied from 2 N·m to 6 N·m, and then back to 4 N·m. From the test results shown in Fig. 20, when the load variations occur, the OLS scheme achieves satisfactory estimation and fast response.

It is known that the DC offset is a serious issue in estimation schemes because even a small DC offset may cause large oscillations in the estimated quantities. To make a performance assessment of the OLS scheme with DC offsets, the corresponding experimental test is conducted, in which the DC offset is set to 0.5 V and 0.3 V, respectively. The results in Fig. 19 demonstrate that the closed-loop flux observer offers good robustness against the DC offsets. Consequently, the estimated rotor flux is immune to the effect of DC offsets, and accordingly, the estimation of the OLS scheme is maintained.

The performance of the OLS scheme with distorted inputs is evaluated through experimental tests, and compared with that of the PLL scheme. In this case, the distortions, consisting of 250 Hz and 350 Hz sinusoidal signals, are introduced into the inputs. And, the amplitudes of these distortions are set to 0.2 V firstly, and then, reduce to 0.1 V. Fig. 20 illustrates the performance of the OLS scheme with distorted inputs. It can be observed in Fig. 20 that the OLS scheme behaves well and the estimation errors are limited in a reasonable range. By comparison, as shown in Fig. 21, the PLL scheme achieves speed estimation with unsatisfactory estimation accuracy. That is, large oscillatory ripples appear in the estimated speed.

Additionally, to highlight the estimation performance of the OLS scheme, a comparison between the OLS scheme and the type-3 PLL scheme is experimentally made, which is shown in Fig. 22. In this case, the speed command is changed from 1000 r/min to 1430 r/min, and then back to 1200 r/min. From the results shown in Fig. 22, both high estimation accuracy and fast dynamics are achieved, when executing the OLS scheme. While, in the type-3 PLL scheme, an oscillatory dynamic response can be observed. More specifically, a large overshoot appears in the estimated speed.

The performance of the speed estimation scheme in the low speed range is of importance. Considering this, the estimation performance of the OLS scheme is explored in a low speed range. In this case, the speed command is set to 100 r/min. Observations in Fig. 23 suggest that the OLS scheme provides an acceptable estimation in this case.

In all, the OLS scheme provides speed estimation with good accuracy under different cases. The SOGI-FLL scheme, nevertheless, presents apparent estimation errors during acceleration and deceleration processes. Moreover, with the assistance of the closed-loop flux observer, the estimation performance of the OLS scheme with DC offsets is guaranteed. Particularly, the OLS scheme shows good estimation performance when distortions appear in the inputs. However, considerable oscillatory ripples can be observed in the estimated speed when implementing the PLL scheme with distorted inputs. Comparisons between the proposed OLS scheme and the type-3 PLL scheme confirm that the OLS scheme is a better option in terms of system dynamics.

2168-6777 (c) 2020 IEEE. Personal use is permitted, but republication/redistribution requires IEEE permission. See http://www.ieee.org/publications_standards/publications/rights/index.html for more information.
Authorized licensed use limited to: Aalborg Universitetsbibliotek. Downloaded on January 15,2021 at 10:27:43 UTC from IEEE Xplore. Restrictions apply.

This article has been accepted for publication in a future issue of this journal, but has not been fully edited. Content may change prior to final publication. Citation information: DOI 10.1109/JESTPE.2021.3050805, IEEE Journal of Emerging and Selected Topics in Power Electronics

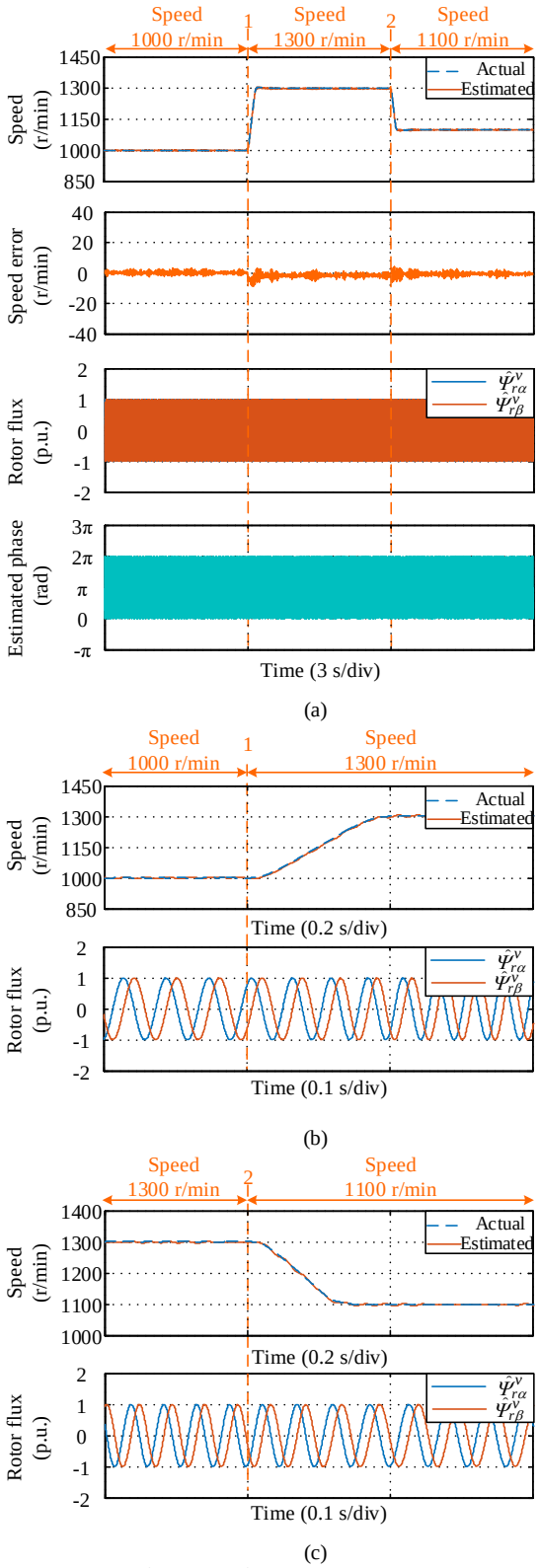

Fig. 15. Estimation performance of the OLS scheme under speed command variations: (a) the estimation performance, (b) the zoom-in 1, and (c) the zoom-in 2.

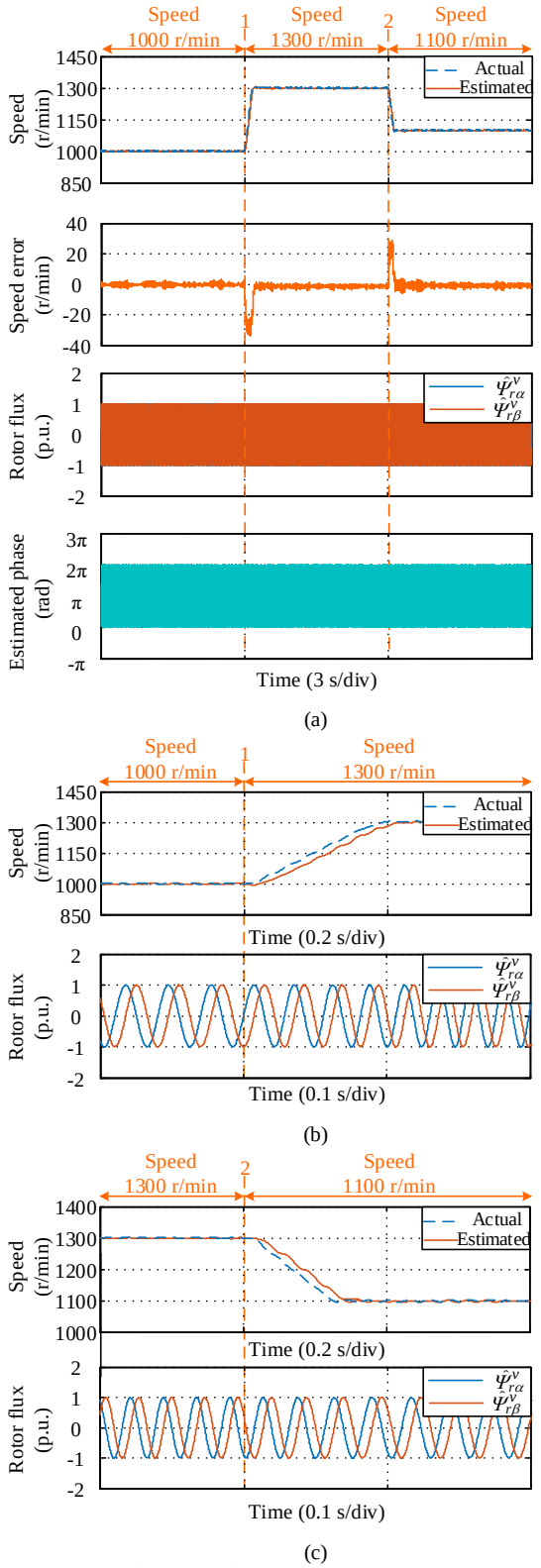

Fig. 16. Estimation performance of the conventional SOGI-FLL scheme under speed command variations: (a) the estimation performance, (b) the zoom-in 1, and (c) the zoom-in 2.

2168-6777 (c) 2020 IEEE. Personal use is permitted, but republication/redistribution requires IEEE permission. See http://www.ieee.org/publications_standards/publications/rights/index.html for more information.
Authorized licensed use limited to: Aalborg Universitetsbibliotek. Downloaded on January 15,2021 at 10:27:43 UTC from IEEE Xplore. Restrictions apply.

This article has been accepted for publication in a future issue of this journal, but has not been fully edited. Content may change prior to final publication. Citation information: DOI 10.1109/JESTPE.2021.3050805, IEEE Journal of Emerging and Selected Topics in Power Electronics

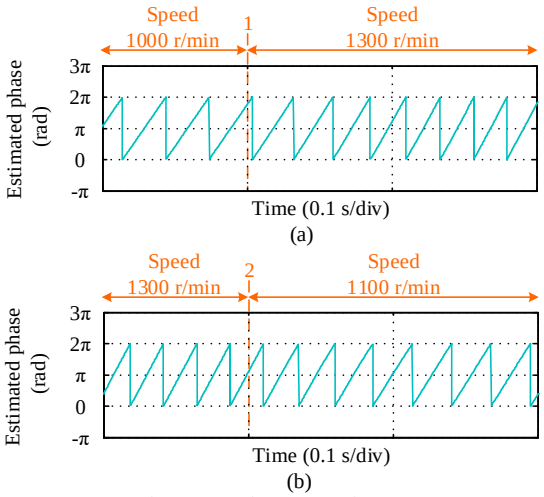

Fig. 17. Estimation performance of the rotor flux phase by using the OLS scheme under speed command variations: (a) the zoom-in 1 of Fig. 15 and (b) the zoom-in 2 of Fig. 15.

VII. Conclusion

The CLS-based speed estimation schemes, e.g., PLL- and SOGI-FLL-based schemes, are preferable in speed-sensorless control of motor drives. However, these schemes may present estimation errors during acceleration and deceleration processes. To improve estimation performance, an attempt by using the type-3 PLL scheme was made. However, this scheme may affect the stability margin and system dynamics. Considering this, a speed estimation scheme with an OLS method was proposed in this paper for speed-sensorless control of induction motor drives. In the proposed OLS scheme, the estimated speed was obtained from the sinusoidal signals and their time-delay signals, rather than solely increasing the system order. In practice, the estimation may be compromised due to DC offsets, and hence, a closed-loop flux observer was employed in the OLS scheme to deal with the DC offsets. The performance of the OLS scheme has been investigated through extensive experimental tests, and compared with that of the prior-art CLS schemes and the type-3 PLL scheme.

References

[1] J. Holtz, "Sensorless control of induction motor drives," *Proc. IEEE*, vol. 90, no. 8, pp. 1359-1394, Aug. 2002.

[2] J. Holtz, "Sensorless control of induction machine—with or without signal injection?" *IEEE Trans. Ind. Electron.*, vol. 53, no. 1, pp. 7-30, Feb. 2006.

[3] C. Caruana, G. M. Ashe, and M. Sumner, "Performance of HF signal injection techniques for zero-low-frequency vector control of induction machines under sensorless conditions," *IEEE Trans. Ind. Electron.*, vol. 53, no. 1, pp. 225-238, Feb. 2006.

[4] Q. Gao, G. Asher, and M. Sumner, "Sensorless position and speed control of induction motors using high-frequency injection and without offline precommissioning," *IEEE Trans. Ind. Electron*., vol. 54, no. 5, pp. 2474-2481, Oct. 2007.

[5] S. Golestan, J. M. Guerrero, and J. C. Vasquez, "Three-phase PLLs: A review of recent advances," *IEEE Trans. Power Electron.*, vol. 32, no. 3, pp. 1894-1907, Mar. 2017.

[6] S. Golestan, J. M. Guerrero, and J. C. Vasquez, "Single-phase PLLs: A review of recent advances," *IEEE Trans. Power Electron*., vol. 32, no. 12, pp. 9013-9030, Dec. 2017.

[7] G. Wang, M. Valla, and J. Solsona, "Position sensorless permanent magnet synchronous machine drives—a review," *IEEE Trans. Ind. Electron.*, vol. 67, no. 7, pp. 5830-5842, Jul. 2020.

[8] G. Wang, R. Yang, and D. Xu, "DSP-based control of sensorless IPMSM drives for wide-speed-range operation," *IEEE Trans. Ind. Electron.*, vol. 60, no. 2, pp. 720-727, Feb. 2013.

[9] G. Wang, T. Li, G. Zhang, X. Gui, and D. Xu, "Position estimation error reduction using recursive-least-square adaptive filter for model based sensorless interior permanent-magnet synchronous motor drives," *IEEE Trans. Ind. Electron*., vol. 61, no. 9, pp. 5115-5125, Sep. 2014.

[10] G. Zhang, G. Wang, D. Xu, and N. Zhao, "ADALINE-network-based PLL for position sensorless interior permanent magnet synchronous motor drives," *IEEE Trans. Power Electron*., vol. 31, no. 2, pp. 1450-1460, Feb. 2016.

[11] G. Zhang, G. Wang, D. Xu, R. Ni, and C. Jia, "Multiple-AVF cross-feedback-network-based position error harmonic fluctuation elimination for sensorless IPMSM drives," *IEEE Trans. Ind. Electron.*, vol. 63, no. 2, pp. 821-831, Feb. 2016.

[12] Q. An, J. Zhang, Q. An, X. Liu, A. Shamekov, and K. Bi, "Frequency-adaptive complex-coefficient filter-based enhanced sliding mode observer for sensorless control of permanent magnet synchronous motor drives," *IEEE Trans. Ind. Appl*., vol. 56, no. 1, pp. 335-343, Jan./Feb. 2020.

[13] S. Golestan, J. M. Guerrero, J. C. Vasquez, A. M. Abusorrah, and Y. A. Turki, "A study on three-phase FLLs," *IEEE Trans. Power Electron.*, vol. 34, no. 1, pp. 213-224, Jan. 2019.

[14] H. Wang, Y. Yang, Y. Zuo, S. Li, X. Hu, and X. Ge, "A speed estimation scheme based on an improved SOGI-FLL for speed-sensorless control of induction motor drives," in *Proc. IECON* 2020, 2020, pp. 852-857.

[15] P. Rodriguez, A. Luna, R. S. M. Aguilar, I. E. Otadui, R. Teodorescu, and F. Blaabjerg, "A stationary reference frame grid synchronization system for three-phase grid-connected power converters under adverse grid conditions," *IEEE Trans. Power Electron*., vol. 27, no. 1, pp. 99-112, Jan. 2012.

[16] Z. Xin, R. Zhao, F. Blaabjerg, L. Zhang, and P. C. Loh, "An improved flux observer for field-oriented control of induction motors based on dual second-order generalized integrator frequency-locked loop," *IEEE J. Emerg. Sel. Top. Power Electron.*, vol. 5, no. 1, pp. 513-525, Mar. 2017.

[17] S. Golestan, J. M. Guerrero, F. Musavi, and J. C. Vasquez, "Single-phase frequency-locked loops: A comprehensive review," *IEEE Trans. Power Electron.*, vol. 34, no. 12, pp. 11791-11812, Dec. 2019.

[18] H. X. Nguyen, T. N. C. Tran, J. W. Park, and J. W. Jeon, "An adaptive linear neuron based third-order PLL to improve the accuracy of absolute magnetic encoders," *IEEE Trans. Ind. Electron.*, vol. 66, no. 6, pp. 4639-4649, Jun. 2019.

[19] H. Wang and X. Ge, "Type-3 PLL based speed estimation scheme for sensorless linear induction motor drives," in *Proc. 10th Int. Conf. Power Electron. ECCE Asia* , May 2019, pp. 1303-1308.

[20] S. Golestan, M. Monfared, F. D. Freijedo, and J. M. Guerrero, "Advantages and challenges of a type-3 PLL," *IEEE Trans. Power Electron.*, vol. 28, no. 11, pp. 4985-4997, Nov. 2013.

[21] M. K. Ghartemani, B. Ooi, and A. Bakhshai, "Application of enhanced phase-locked loop system to the computation of synchrophasors," *IEEE Trans. Power Del.*, vol. 26, no. 1, pp. 22-32, Jan. 2011.

[22] B. I. Rani, C. K. Aravind, G. S. Ilango, and C. Nagamani, "A three phase PLL with a dynamic feed forward frequency estimator for synchronization of grid connected converters under wide frequency variations," *Int. J. Elect. Power Energy Syst.*, vol. 41, no. 1, pp. 63-70, Oct. 2012.

[23] F. Liccardo, P. Marino, and G. Raimondo, "Robust and fast three-phase PLL tracking system," *IEEE Trans. Ind. Electron.*, vol. 58, no. 1, pp. 221-231, Jan. 2011.

[24] S. Golestan, M. Ramezani, and J. M. Guerrero, "An analysis of the PLLs with secondary control path," *IEEE Trans. Ind. Electron.*, vol. 61, no. 9, pp. 4824-4828, Sep. 2014.

[25] H. Wang, X. Ge, Y. Yue, and Y. Liu, "Dual phase-locked loop based speed estimation scheme for sensorless vector control of linear induction motor drives," *IEEE Trans. Ind. Electron*., vol. 67, no. 7, pp. 5900-5912, Jul. 2020.

2168-6777 (c) 2020 IEEE. Personal use is permitted, but republication/redistribution requires IEEE permission. See http://www.ieee.org/publications_standards/publications/rights/index.html for more information.
Authorized licensed use limited to: Aalborg Universitetsbibliotek. Downloaded on January 15,2021 at 10:27:43 UTC from IEEE Xplore. Restrictions apply.

This article has been accepted for publication in a future issue of this journal, but has not been fully edited. Content may change prior to final publication. Citation information: DOI 10.1109/JESTPE.2021.3050805, IEEE Journal of Emerging and Selected Topics in Power Electronics

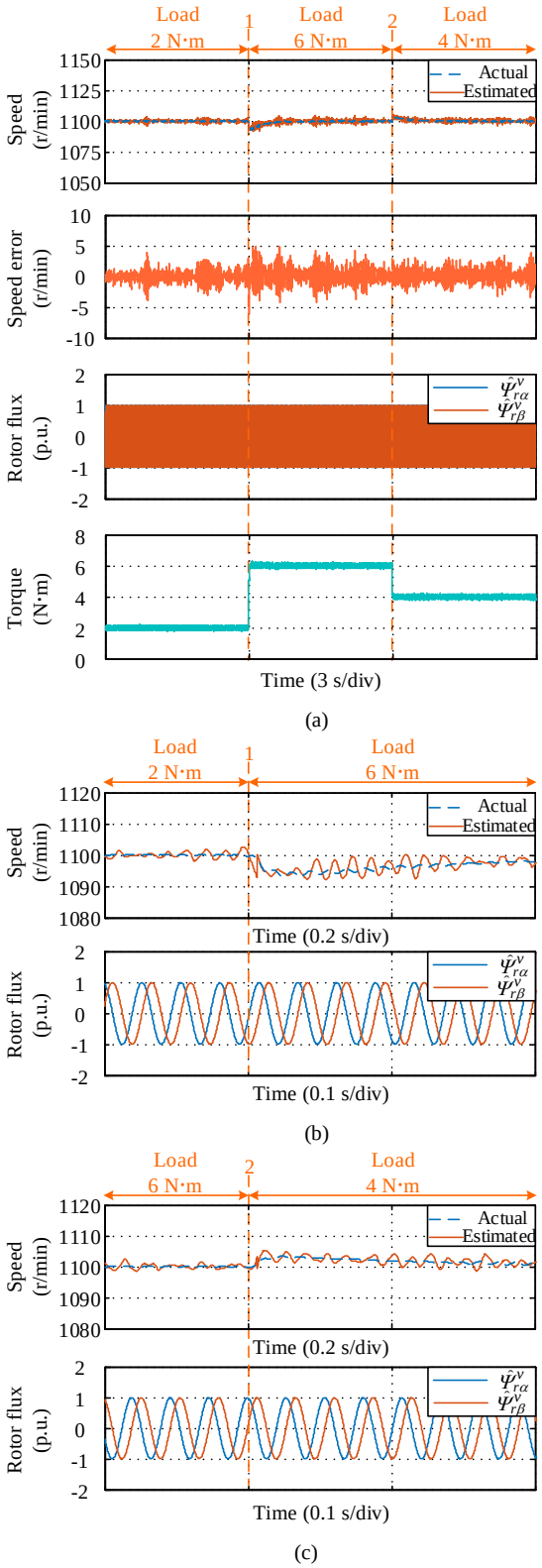

Fig. 18. Estimation performance of the OLS scheme under load variations: (a) the estimation performance, (b) the zoom-in 1, and (c) the zoom-in 2.

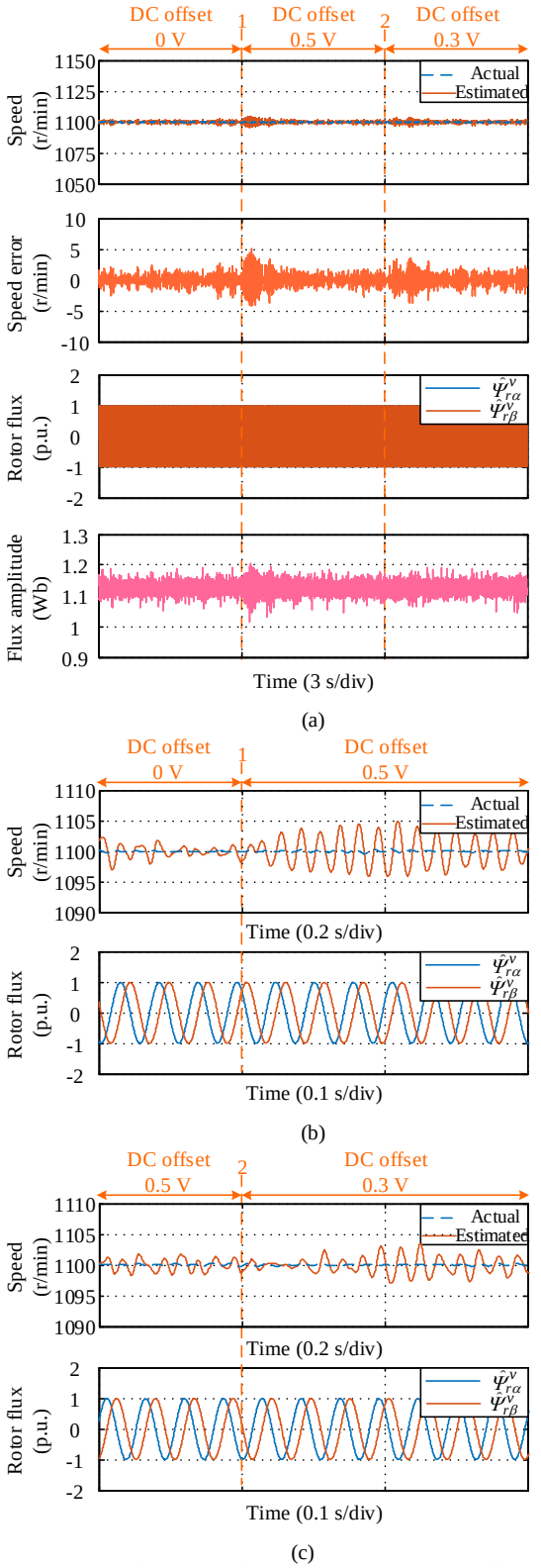

Fig. 19. Estimation performance of the OLS scheme with DC offsets: (a) the estimation performance, (b) the zoom-in 1, and (c) the zoom-in 2.

2168-6777 (c) 2020 IEEE. Personal use is permitted, but republication/redistribution requires IEEE permission. See http://www.ieee.org/publications_standards/publications/rights/index.html for more information.
Authorized licensed use limited to: Aalborg Universitetsbibliotek. Downloaded on January 15,2021 at 10:27:43 UTC from IEEE Xplore. Restrictions apply.

This article has been accepted for publication in a future issue of this journal, but has not been fully edited. Content may change prior to final publication. Citation information: DOI 10.1109/JESTPE.2021.3050805, IEEE Journal of Emerging and Selected Topics in Power Electronics

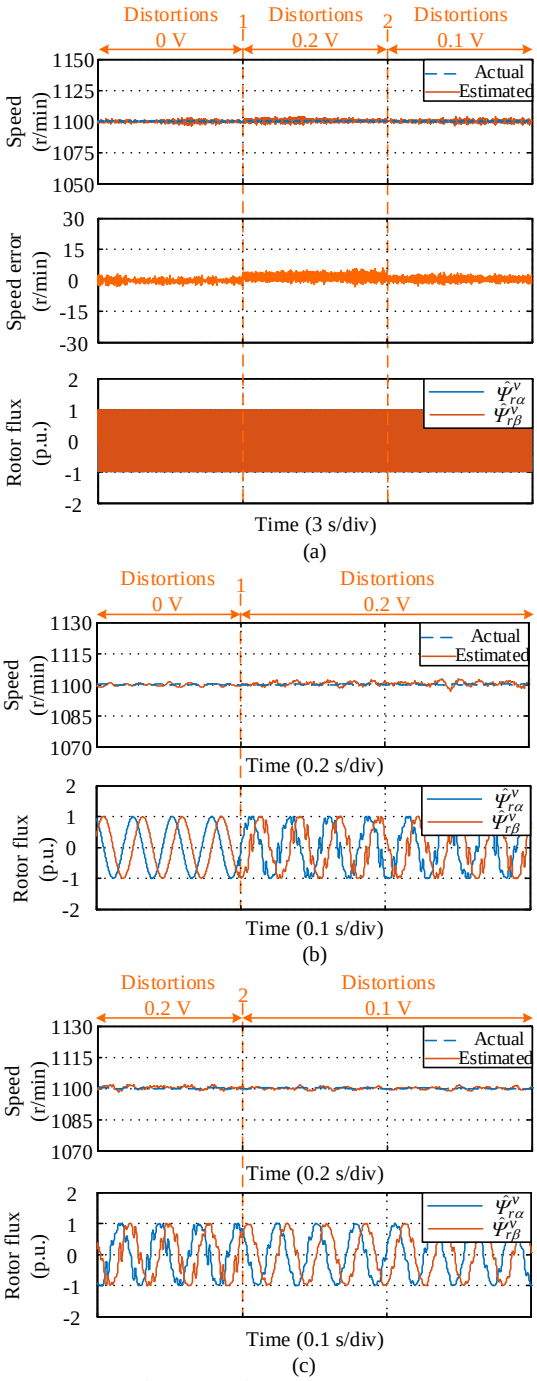

Fig. 20. Estimation performance of the OLS scheme with distortions in the inputs: (a) the estimation performance, (b) the zoom-in 1, and (c) the zoom-in 2.

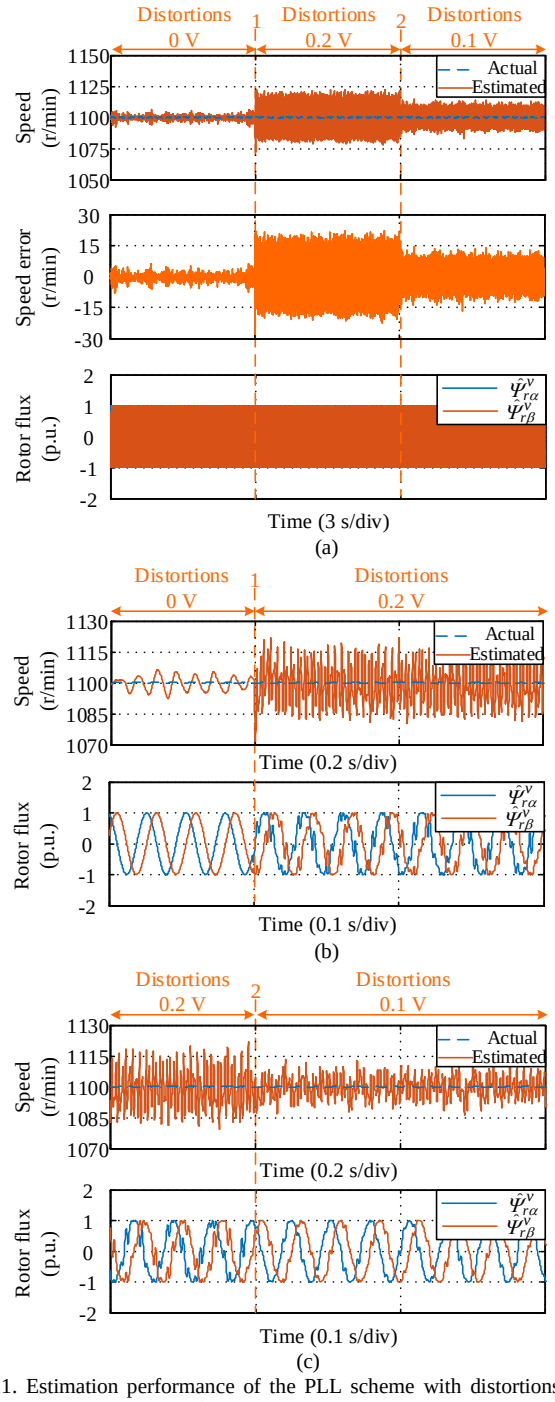

Fig. 21. Estimation performance of the PLL scheme with distortions in the inputs: (a) the estimation performance, (b) the zoom-in 1, and (c) the zoom-in 2.

[26] H. Machida, M. Kambara, K. Tanaka, and F. Kobayashi, "A motor speed control system using a hybrid of dual-loop PLL and feed-forward," in *Proc. Int. Workshop Adv. Motion Control AMC*, pp. 185-190, Mar. 2010.

[27] H. Mchida, M. Kambara, K. Tanaka, and F. Kobayashi, "A motor speed control system using dual-loop PLL and speed feed-forward/back," in *Proc. IEEE Int. Conf. Mechatron. Autom.*, Aug. 2010, pp. 1512-1517.

[28] H. Wang, Y. Yang, X. Ge, S. Li, and Y. Zuo, "Speed-sensorless control of linear induction motor based on the SSLKF-PLL speed estimation scheme," *IEEE Trans. Ind. Appl.*, vol. 56, no. 5, pp. 4896-5002, Sep./Oct. 2020.

[29] S. Golestan, J. M. Guerrero, and J. C. Vasquez, "Steady-state linear Kalman filter-based PLLs for power applications: A second look," *IEEE Trans. Ind. Electron.*, vol. 65, no. 12, pp. 9795-9800, Dec. 2018.

[30] H. A. Hamed and M. S. E. Moursi, "A new type-2 PLL based on unit delay phase angle error compensation during the frequency ramp," *IEEE Trans. Power Syst.*, vol. 34, no. 4, pp. 3289-3293, Jul. 2019.

[31] H. Albeshr, M. S. E. Moursi, H. A. Hamed, and A. S. A. Sumaiti, "Advanced type-1c FLL for enhancing converters synchronization during frequency drift," *IEEE Trans. Power Del.*, 2020, early access, doi: 10.1109/TPWRD.2020.3001217.

2168-6777 (c) 2020 IEEE. Personal use is permitted, but republication/redistribution requires IEEE permission. See http://www.ieee.org/publications_standards/publications/rights/index.html for more information.
Authorized licensed use limited to: Aalborg Universitetsbibliotek. Downloaded on January 15,2021 at 10:27:43 UTC from IEEE Xplore. Restrictions apply.

This article has been accepted for publication in a future issue of this journal, but has not been fully edited. Content may change prior to final publication. Citation information: DOI 10.1109/JESTPE.2021.3050805, IEEE Journal of Emerging and Selected Topics in Power Electronics

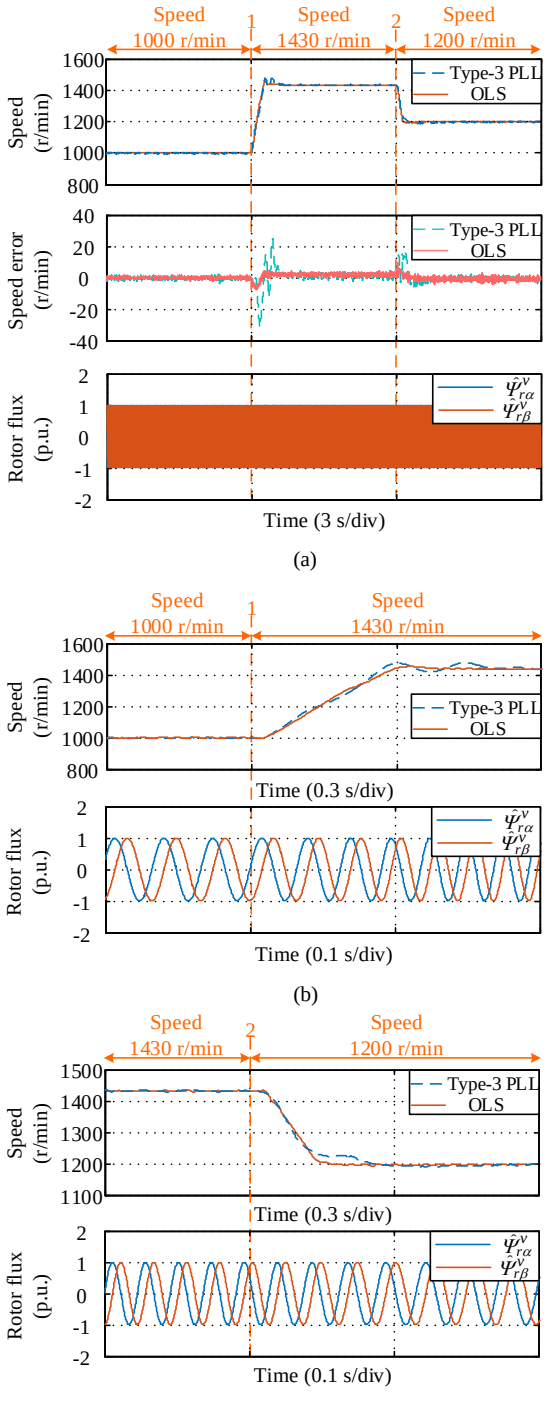

Fig. 22. Estimation performance comparison between the OLS scheme and the type-3 PLL scheme under speed command variations: (a) the entire estimation performance comparison, (b) the zoom-in 1, and (c) the zoom-in 2.

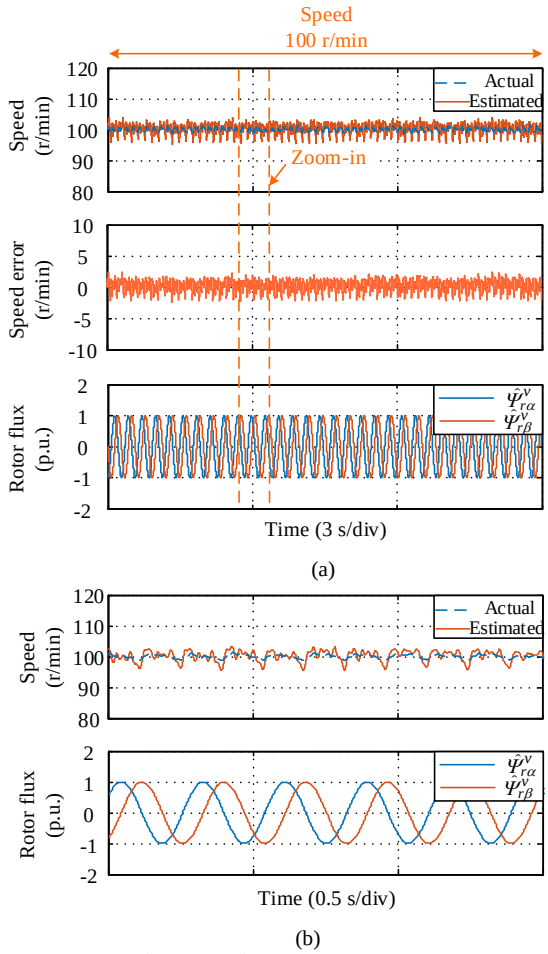

Fig. 23. Estimation performance of the OLS scheme in a low speed range: (a) the estimation performance and (b) the zoom-in area.

[32] S. Golestan, A. Vidal, A. G. Yepes, J. M. Guerrero, J. C. Vasquez, and J. Doval-Gandoy, "A true open-loop synchronization technique," *IEEE Trans. Ind. Inform.*, vol. 12, no. 3, pp. 1093-1103, Jun. 2016.

[33] F. Xiao, L. Dong, L. Li, and X. Liao, "A novel open-loop frequency estimation method for single-phase grid synchronization under distorted conditions," *IEEE J. Emerg. Sel. Top. Power Electron.*, vol. 5, no. 3, pp. 1287-1297, Sep. 2017.

[34] M. S. Reza, M. Ciobotaru, and V. G. Agelidis, "A robust frequency estimation technique based on three consecutive samples for single-phase systems," *IEEE J. Emerg. Sel. Top. Power Electron.*, vol. 2, no. 4, pp. 1049-1058, Dec. 2014.

[35] S. Golestan, J. M. Guerrero, and J. C. Vasquez, "An open-loop grid synchronization approach for single-phase applications," *IEEE Trans. Power Electron.*, vol. 33, no. 7, pp. 5548-5555, Jul. 2018.

[36] Z. Dai, M. Fan, H. Nie, J. Zhang, and J. Li, "A robust frequency estimation method for aircraft grids under distorted conditions," *IEEE Trans. Ind. Electron.*, vol. 67, no. 5, pp. 4254-4258, May 2020.

[37] A. K. Verma, R. K. Jarial, P. R. Sanchez, M. R. Ungarala, and J. M. Guerrero, "An improved hybrid pre-filtered open-loop algorithm for three-phase grid synchronization," *IEEE Trans. Ind. Electron.*, vol. 68, no. 3, pp. 2480-2490, Mar. 2021.

[38] J. Chen and J. Huang, "Alternative solution regarding problems of adaptive observer compensating parameters uncertainties for sensorless induction motor drives," *IEEE Trans. Ind. Electron.*, vol. 67, no. 7, pp. 5879-5888, Jul. 2020.

[39] G. Tao, *Adaptive Control Design and Analysis*. Hoboken, NJ, USA: Wiley, 2003.

[40] C. Lascu, I. Boldea, and F. Blaabjerg, "A modified direct torque control for induction motor sensorless drive," *IEEE Trans. Ind. Appl.*, vol. 36, no. 1, pp. 122-130, Jan./Feb. 2000.

2168-6777 (c) 2020 IEEE. Personal use is permitted, but republication/redistribution requires IEEE permission. See http://www.ieee.org/publications_standards/publications/rights/index.html for more information.
Authorized licensed use limited to: Aalborg Universitetsbibliotek. Downloaded on January 15,2021 at 10:27:43 UTC from IEEE Xplore. Restrictions apply.

This article has been accepted for publication in a future issue of this journal, but has not been fully edited. Content may change prior to final publication. Citation information: DOI 10.1109/JESTPE.2021.3050805, IEEE Journal of Emerging and Selected Topics in Power Electronics

Huimin Wang (S'17) received the B.Eng. degrees in electrical engineering from Southwest Jiaotong University (SWJTU), Chengdu, China, in 2016. He is currently working toward the Ph.D. degree in electrical engineering at the Southwest Jiaotong University, Chengdu, China.

His research interests include induction motor drive system and its speed-sensorless control, and synchronization technique in grid-connected system.

Mr. Wang was a recipient of the Best Paper Award of IEEE Transportation Electrification Conference and EXPO Asia-Pacific (ITEC Asia-Pacific) in 2019.

Yongheng Yang (SM'17) received the B.Eng. degree from Northwestern Polytechnical University, China, in 2009 and the Ph.D. degree from Aalborg University, Denmark, in 2014. He was a postgraduate student with Southeast University, China, from 2009 to 2011. In 2013, he spent three months as a Visiting Scholar at Texas A&M University, USA. Since 2014, he has been with the Department of Energy Technology, Aalborg University, where he became a tenured Associate Professor in 2018. In January 2021, he joined Zhejiang University, China, where he is now a Professor (tenure-track) at the Department of Electrical Engineering.

Dr. Yang was the Chair of the IEEE Denmark Section (2019-2020). He is an Associate Editor for several IEEE Transactions/Journals. He is a Deputy Editor of the IET Renewable Power Generation for Solar Photovoltaic Systems. He was the recipient of the 2018 IET Renewable Power Generation Premium Award and was an Outstanding Reviewer for the IEEE TRANSACTIONS ON POWER ELECTRONICS in 2018. In addition, he has received two IEEE Best Paper Awards. His current research includes the grid-integration of photovoltaic systems and multi-energy vectors with an emphasis on power converter design, control, and reliability.

Dunzhi Chen (S'19) received the B.S. degree from Jiangsu University of Science and Technology, Zhangjiagang, China, in 2015, and the M.S. degree from Shanghai Maritime University, Shanghai, China, in 2017, all in electrical engineering. He is now working toward a Ph.D. degree in the Department of Energy Technology, Aalborg University, Aalborg, Denmark.

His current research interest is sensorless control of permanent magnet synchronous machines.

Xinglai Ge (M'15) received the B.S., M.S., and Ph.D. degrees in electrical engineering from Southwest Jiaotong University (SWJTU), Chengdu, China, in 2001, 2004, and 2010, respectively. He is currently a Full Professor in the School of Electrical Engineering, Southwest Jiaotong University and a Vice Director of Department of Power Electronics and Power Drive.

From July to August of 2012, he was a visiting scholar at George Mason University, VA, USA. From October 2013 to October 2014, he was a visiting scholar at the School of Electrical and Computer Engineering, Georgia Institute of Technology, Atlanta, GA, USA. He is the author and co-author of more than 60 technical papers

His research interests include stability analysis and control of electrical traction system, fault diagnosis and reliability of traction converter and motor drive system.

Songtao Li received the B.Eng. degree in electrical engineering from the Lanzhou University of Technology, Lanzhou, China, in 2018. He is currently pursuing the M.Eng. degree in power electronics and electrical drives with the School of Electrical Engineering, Southwest Jiaotong University, Chengdu, China.

His current research interests include permanent magnet synchronous motor drives and position sensorless control.

Zuo Yun (S'20) received the B.Eng. degree in electrical engineering and automation from Dalian Jiaotong University, Dalian, China, in 2019. He is currently pursuing the M.Eng. degree in electrical engineering with Southwest Jiaotong University, Chengdu, China.

His research interests include induction motor drive systems and its speed-sensorless control.

2168-6777 (c) 2020 IEEE. Personal use is permitted, but republication/redistribution requires IEEE permission. See http://www.ieee.org/publications_standards/publications/rights/index.html for more information.
Authorized licensed use limited to: Aalborg Universitetsbibliotek. Downloaded on January 15,2021 at 10:27:43 UTC from IEEE Xplore. Restrictions apply.